Nicolas Chevigny[1], Cédric Nadiras[1], Cécile Raynaud[2], Monique Le Ret[1], Marc Bichara[2], Mathieu Erhardt[1], André Dietrich[1] and José M. Gualberto[1]

[1]Institut de Biologie Moléculaire des Plantes, CNRS UPR2357, Université de Strasbourg, 12 rue du General Zimmer, 67084 Strasbourg, France

[2]Institute of Plant Sciences Paris-Saclay (IPS2), CNRS, INRA, Université Paris-Sud, Université Evry, Université Paris-Saclay, 91405, Orsay, Paris, France
S1

[3]CNRS UMR7242, IREBS, Université de Strasbourg, Bld Sébastien Brandt BP 10413, 67412 Illkirch, France

***Corresponding author:**

José M. Gualberto

Institut de Biologie Moléculaire des Plantes, CNRS, Université de Strasbourg
12 rue du General Zimmer, 67084 Strasbourg, France
Tel (+33) 367155361
Fax (+33) 3 67 15 53 00
jose.gualberto@ibmp-cnrs.unistra.fr

Title:

RADA is the main branch migration factor in plant mitochondrial recombination and its defect leads to mtDNA instability and cell cycle arrest

Short title: RADA in mitochondrial genome stability

The author responsible for distribution of materials integral to the findings presented in this article in accordance with the policy described in the Instructions for Authors (www.plantcell.org) is José M. Gualberto (jose.gualberto@ibmp-cnrs.unistra.fr).

SYNOPSIS

Arabidopsis RADA is a main branch migration activity in plant mitochondria, whose deficiency leads to mtDNA instability by recombination, and suppression of plant growth by the activation of repressors of cell cycle progression.

ABSTRACT

The mitochondria of flowering plants have large and complex genomes whose structure and segregation are modulated by recombination activities. Among unresolved questions is what are the pathways responsible for the late steps of homologous recombination: while the loss of mitochondrial recombination is not viable, a deficiency in RECG1-dependent branch migration has little impact on plant development. Here we present an additional pathway required for the processing of organellar recombination intermediates, the one depending on *RADA*. RADA is similar in structure and activity to bacterial RadA/Sms, and in vitro it binds to ssDNA and accelerates strand-exchange reactions initiated by RecA. RADA-deficient plants are severely impacted in their development and fertility, correlating with increased mtDNA ectopic recombination and replication of recombination-generated subgenomes. The *radA* mutation is epistatic to *recG1*, indicating that RADA drives the main branch migration pathway of plant mitochondria. In contrast, the double mutation *radA recA3* is lethal, revealing the importance of an alternative RECA3-dependent pathway. Interestingly, the *radA* developmental phenotypes could not be correlated with obvious defects in mitochondrial gene expression. Rather, it seems that it is the activation of genes that repress cell cycle progression that is partially the cause of the stunted growth of *radA* mutants.

INTRODUCTION

The mitochondrial genomes (mtDNA) of vascular plants are large and complex, mostly consisting of non-coding sequences assembled in a heterogeneous population of linear, circular and branched double-stranded (dsDNA) or single-stranded (ssDNA) DNA molecules (Backert et al., 1997; Bendich, 1996; Manchekar et al., 2006). In most species this collection of subgenomic molecules can be mapped into a single circular chromosome, but multichromosome mitogenomes can also exist (Sloan, 2013). The complexity of the plant mtDNA comes from frequent homologous recombination (HR) events involving repeated sequences. Large repeated sequences (> 500 bp) are involved in frequent and reversible homologous recombination (HR), while intermediate-size repeats (IRs) (50-500 bp) or microhomologies (<50 bp) can promote infrequent ectopic or illegitimate recombination, respectively (Christensen, 2018; Gualberto and Newton, 2017; Maréchal and Brisson, 2010; Woloszynska and Trojanowski, 2009). Recombination involving IRs or microhomologies contributes to the heteroplasmic state of mtDNA by creating sub-stoichiometric alternative configurations (mitotypes) that co-exist with the main genome (Small et al., 1989). Sub-stoichiometric mtDNA variants can become the predominant genome by a yet unclear process of clonal expansion called sub-stoichiometric shifting that can occur in the time frame of a single plant generation (Janska et al., 1998; Small et al., 1989; Vitart et al., 1992). These variants may present altered gene expression, resulting from the displacement of regulatory sequences or from the disruption of gene sequences. Such events may lead to the creation and expression of chimeric ORFs that can be deleterious for mitochondrial function, like in the case of cytoplasmic male sterility (CMS) (Budar et al., 2003; Hanson and Bentolila, 2004). HR is also the main DNA repair pathway of plant mitochondria, for the repair of double strand breaks (DSBs) and the copy-correction of mutations, thus contributing to the very slow evolution of plant mtDNA coding sequences (Christensen, 2013; Mower et al., 2007).

Many of the factors involved in plant organellar recombination pathways are derived from prokaryotic homologs inherited from the symbiotic ancestors of mitochondria and chloroplasts (Boesch et al., 2011; Gualberto and Newton, 2017). However, the organellar pathways can significantly depart from the ones of their bacterial counterparts, and involve additional factors with partially redundant functions. As a representative example, plant organellar recombination relies on the abundant RecA-like RECA2 recombinase (about 450 copies/mitochondrion, Fuchs et al., 2019), which is targeted to both organelles and whose mutation is lethal at the seedling developmental stage (Miller-Messmer et al., 2012; Shedge et al., 2007), but also involves plastidial RECA1 and mitochondrial RECA3. Although it could not be detected in Arabidopsis cultured cells (Fuchs et al., 2019) RECA3 is critical for mtDNA maintenance, since its loss causes mtDNA instability that worsens over generations (Miller-

Messmer et al., 2012; Shedge et al., 2007). This possibly reflects specialized functions and expression of RECA3 in specific tissues such as gametophytes (Miller-Messmer et al., 2012). Defect in the factors involved in mitochondrial HR generally results in genomic rearrangements because of increased ectopic recombination, a consequence of enhanced activity of alternative error-prone repair pathways (Miller-Messmer et al., 2012; Wallet et al., 2015).

In bacteria, HR is initiated by the loading of RecA on ssDNA, forming a nucleofilament that then seeks for homologies in the genome by probing multiple heterologous sequences (Forget and Kowalczykowski, 2012; Ragunathan et al., 2012). When a homologous sequence is identified, RecA-mediated ATP hydrolysis stabilizes the invading DNA, forming the synaptic complex also known as displacement loop or D-loop. An important post-synaptic step is branch migration, which involves helicases that extend the homologous region on both sides of the D-loop, allowing the recruitment of the fourth DNA strand to form a Holliday Junction (Cooper and Lovett, 2016; West, 1997; Whitby et al., 1994). Three partially redundant pathways of branch migration have been described in bacteria, involving RuvAB, RecG and RadA, respectively (Beam et al., 2002; Cooper et al., 2015). RadA has long been known as a RecA-like factor influencing repair by recombination (Beam et al., 2002), but its biochemical activities were only recently characterized (Cooper and Lovett, 2016; Marie et al., 2017). It is an ATP-dependent ssDNA helicase composed of three functional domains: an N-terminal C4 zinc-finger, a RecA-like ATPase domain and a Lon protease-like domain (Cooper et al., 2015). In contrast to RecG and RuvAB, RadA interacts with RecA and can function in the context of the RecA nucleofilament. Bacterial *radA* or *recG* single mutants are only mildly affected, but the *radA recG* double mutant is severely impaired in its survival under genotoxic conditions (Cooper et al., 2015). In fact, highlighting the crucial role of branch migration in HR, the deficiency in multiple branch migration pathways is more deleterious to the cell than the absence of recombination, probably because of the accumulation of toxic unprocessed recombination intermediates, (Beam et al., 2002; Cooper et al., 2015).

Plant genomes do not encode any homolog of the RuvAB complex, but code for a RecG homolog (RECG1) involved in mitochondrial recombination (Wallet et al., 2015; Odahara et al., 2015). Despite the absence of a mitochondrial RuvAB pathway, Arabidopsis *recG1* mutants are only mildly affected. As organellar recombination is essential for plant development (Miller-Messmer et al., 2012), a more deleterious effect was expected for the loss of this branch migration activity, suggesting the existence of additional pathways for the maturation of recombination intermediates.

Here we describe a plant RadA homolog that could potentially be involved in the late steps of organellar HR pathways. We show that Arabidopsis RADA possesses similar

activities as bacterial RadA. However, contrarily to bacteria, plant *radA* mutants are severely affected in their development because of mtDNA instability. The mutation is epistatic to *recG1,* indicating that RADA has a more prominent role in plant mitochondrial recombination than it has in bacteria. Furthermore we found that mtDNA instability triggered by the deficiency of RADA activates genes involved in the suppression of cell cycle progression, partially explaining the growth defect of *radA* plants.

RESULTS

All plant genomes encompass a gene coding for RADA, and RADA from Arabidopsis is targeted to both mitochondria and chloroplasts

In bacteria, the *recG* mutation is strongly synergetic with *radA* for the repair of DNA damages, and the double mutant *recG radA* is at least as affected in growth as the RecA-deficient *recA* mutant (Beam et al., 2002; Cooper et al., 2015). In Arabidopsis mitochondria, RECA-dependent recombination is essential (Miller-Messmer et al., 2012), but the loss of the organellar-targeted RECG1 has only mild effects on plant fitness (Wallet et al., 2015). This suggested that additional genes exist coding for redundant or overlapping functions, such as for RadA and RecG in bacteria. The Arabidopsis (*Arabidopsis thaliana*) genome was screened for orthologs of RadA and the At5g50340 gene was identified as coding for a protein remarkably similar to bacterial RadA (45 % similarity), which we named *RADA*.

Phylogenetic analysis showed that genes coding for RADA are present in all groups of the green lineage, including land plants, green and red algae, as well as in brown algae, diatoms and also in several organisms of the Stramenopile group that are not photosynthetic, such as the water mold *Phytophtora infestans* (Supplemental Figure 1). But no RADA ortholog was found in animals or in yeast. While it is probable that plants inherited *RADA* from the prokaryote ancestor of mitochondria or chloroplasts, the strong conservation of the sequences did not allow us to infer whether the ancestor was a proteobacterial or a cyanobacterial RadA. Sequence alignments (Supplemental Figure 2) showed that plant RADA proteins have all the important functional motifs that have been described in bacterial RadA (Cooper and Lovett, 2016; Marie et al., 2017). In addition, plant RADA sequences have non-conserved N-terminal extensions predicted to be organellar targeting peptides (http://suba.plantenergy.uwa.edu.au). This assumption was tested by expression of a fusion to GFP. The fusion protein was constitutively expressed in transgenic Arabidopsis plants and found targeted to both chloroplasts and mitochondria, as shown by co-localization with the auto-fluorescence of chlorophyll and the red fluorescence of MitoTracker® (Figure 1). Thus,

RADA is apparently a dually targeted organellar protein, like RECG1 and many other factors involved in maintenance of organellar genomes (Gualberto and Newton, 2017). A previous report described the rice RadA ortholog as targeted to the nucleus (Ishibashi et al., 2006). This was inferred from immunodetection with an antibody supposed to be specific for the recombinant protein. However, our results did not show any hint of a nuclear localization of RADA in Arabidopsis.

Structural and functional conservation of plant RADA as compared to bacterial RadA

Plant RADA has the same modular structure as bacterial RadA (Figure 2A). A three dimensional model of Arabidopsis RADA could be generated (Figure 2B), based on the known structure of *Streptococcus pneumoniae RadA* (Marie et al., 2017). The RadA structure comprises a N-terminal C4 zinc-finger, required for the interaction with RecA, and two main domains: a RecA-like ATPase domain and a Lon protease-like domain. The RecA-like ATPase domain comprises the Walker A and B motifs, and a RadA-specific KNRFG sequence (Figures S2 and 2A). The Walker A and KNRFG motifs are indispensable for the branch migration function of the protein, and are also involved in the DNA-binding and helicase activities of RadA (Cooper and Lovett, 2016; Marie et al., 2017). In bacteria, Walker A and KNRFG mutants are dominant negative, interfering with the function of the wild-type protein. The structural similarity between RadA and RecA suggests functional similarities, but while RecA specialized in the recognition of homologous sequences and strand invasion, RadA rather evolved for driving branch migration. Finally, the C-terminal P-domain of RadA is similar to the Lon protease-like domain of RecA, but it is an inactive domain, since the residues involved in protease activity are not conserved, and no protease activity could be detected (Inoue et al., 2017). Rather, this domain is involved in the binding to dsDNA and it works as a scaffold for the protein architecture, promoting its oligomerization as hexameric rings (Inoue et al., 2017; Marie et al., 2017).

Since all domains of plant RADA match the bacterial ones, it is expected to have the same activities as the bacterial enzyme. We have therefore tested the ability of plant RADA to complement *Escherichia coli* RadA in the repair of genotoxic stress-induced DNA lesions. A *radA785(del)::kan* strain was used for complementation assays, and Arabidopsis RADA and bacterial RadA were expressed from the low-copy number plasmid pACYC. As described by others, we found that the *radA* strain was little affected by genotoxic treatments versus WT (Beam et al., 2002; Cooper et al., 2015). The conditions we found best to test complementation were in the presence ciprofloxacin, an inhibitor of gyrase that induces DNA DSBs. In a spot assay, the growth of radA-deficient cells was much reduced as compared to WT ones. Expression of Arabidopsis RADA could complement the ciprofloxacin-triggered growth defect as well as bacterial RadA cloned in the same expression vector (Figure 2C).

Therefore plant RADA can functionally substitute bacterial RadA in the repair of DNA damages induced by ciprofloxacin.

RADA is an ssDNA-binding protein that stimulates branch migration in strand-exchange reactions

To test plant RADA activities we expressed a recombinant protein in bacteria. The Arabidopsis cDNA sequence minus the first 45 codons coding for the putative organellar targeting sequence was cloned in expression vector pET28a, fused to an N-terminal His-tag. A mutant sequence was prepared to express a Walker A-deficient protein (K201A). The mutation of the equivalent position in *E. coli* RadA abolished DNA-dependent ATPase activity and generated a dominant negative *radA* allele (Cooper et al., 2015; Cooper and Lovett, 2016). According to the structure of the protein bound to ADP the mutation should not affect ATP or ADP binding, even if the ATPase activity is lost (Supplemental Figure 3).

Both WT RADA and K201A could be expressed and purified as soluble proteins (Supplemental Figure 4A). By gel filtration the purified WT protein resolved as two peaks of high molecular weight (Supplemental Figure 4B), indicating different degrees of protein oligomerization. Dynamic light scattering analysis of the smaller size oligomer showed that it was mainly constituted by a monodispersed particle of about 340 kDa, consistent with a hexameric RADA complex (Supplemental Figure 4C). EMSA experiments showed that both peak fractions could bind to an ssDNA oligonucleotide probe and give rise to complexes of same apparent size, but fractions of peak 1 generated predominantly higher molecular weight complexes (Supplemental Figure 4B).

The purified proteins were tested in EMSA experiments with different DNA structures as substrates, including ssDNA, dsDNA, fork-like structures and double-strand molecules containing 5' or 3' ssDNA overhangs. Using the same probe concentrations and increasing concentrations of recombinant protein we found that RADA could bind with equivalent affinities to all structures containing ssDNA regions. Binding to dsDNA also occurred, but with much less affinity (Figure 3A). In competition experiments poly-T, poly-C and poly-G could compete binding as efficiently as the homologous probe, while poly-A was much less efficient as a competitor (Supplemental Figure 5). Thus, Arabidopsis RADA binds preferentially to ssDNA, with little sequence specificity, and apparently without the requirement for ATP or ADP. However, in our experiments we found that higher molecular weight complexes could be formed. These were labile during electrophoresis, and could not be well resolved in standard conditions used for lower molecular weigh complexes. On 4.5 % polyacrylamide gels and at lower voltage we could resolve these complexes, and found that they were promoted by the presence of ATP or ADP (Figure 3B). Such higher molecular weight complexes could correspond to the polymerization of RADA on ssDNA, forming

nucleofilaments. We did not see significant differences in binding with the K201A mutant protein, which seemed to bind to ssDNA with equivalent affinity as the WT protein.

The branch migration activity of plant RADA was also tested, using an *in vitro* strand-exchange reaction promoted by bacterial RecA. RecA, in the presence of ATP and bacterial single-strand binding protein SSB, can initiate the invasion of dsDNA by homologous ssDNA and promote branch migration till the final heteroduplex product is completed. In the presence of plant RADA the branched intermediates were resolved faster, leading to an earlier appearance of the final nicked double-stranded circular product (Figure 3C). The faster resolution of recombination intermediates was reproducibly observed in six independent experiments (Figure 3D).

To test whether RADA-promoted branch migration requires the interaction of the protein with RecA, assays were arrested by freezing at a time point (7 min) when there was already accumulation of branched intermediates, but no visible final heteroduplex product (Figure 3E left panel). The reaction mix was deproteinated and the purified nucleic acids added to new reaction mixes, in the presence or absence of RADA. In the absence of both RecA and RADA the branched intermediates could not spontaneously evolve and remained stable (Figure 3E middle panel), but in the presence of RADA they were converted to the final product, showing that RADA alone can promote branch migration (Figure 3E right panel). However, RADA is not a recombinase redundant with RecA, because RADA alone in the absence of RecA is not able to initiate the strand-invasion reaction (Figure 3F). Finally, in the same experimental conditions the K201A mutant protein was unable to promote branch migration, and rather completely inhibited the reaction (Figure 3G). This could be because of competition with RecA for DNA binding and because of the incapacity of the mutant protein to migrate along the heteroduplexes, an activity dependent on ATP hydrolysis.

Arabidopsis plants deficient in RADA are severely affected in their development

We could retrieve several potential *radA* loss-of-function (KO) lines from available Arabidopsis T-DNA insertion collections, from which two (*radA-1* and *radA-2*) could be confirmed by genotyping and sequencing, with T-DNA insertions in exons 8 and 5 respectively (Figure 4A). Both lines are in the Col-0 background. As compared to WT, homozygous plants from both mutant lines displayed severe phenotypes of retarded growth of both leaves and roots, and of distorted leaves showing chlorotic sectors (Figure 4B-D). The phenotype was fully penetrant, with all homozygous mutants displaying the phenotype. Transmission electron microscope (TEM) observation showed that *radA* mesophyll cells were almost indistinguishable from WT, with chloroplasts that were morphologically normal. On the other hand, mitochondria looked enlarged in size, and less electron dense as compared to those from WT leaves, suggesting that it is the mitochondrion that is

predominantly affected in *radA* (Supplemental Figure 6). The severe dwarf phenotype could be partially relieved by growing *radA* plants on a short day photoperiod (8h light/16h dark, as compared to the 16h light/8h dark standard long day growth conditions). In such conditions plants revealed extended juvenility, with dramatic elongation of lifespan and development of aerial rosettes. Similar phenotype of perennial growth under short days was described for Arabidopsis *msh1* mutants, deficient in the homolog of bacterial mismatch repair protein MutS, and apparently as result from a developmental reprogramming triggered by the chloroplast (Xu et al., 2012).

To fully confirm that these phenotypes were because of a deficiency in RADA, *radA-1* plants were complemented with the WT *RADA* gene expressed under its own promoter. In the T2 generation, homozygous *radA-1* plants that also contained WT *RADA* as a transgene were phenotypically normal (Figure 4B), confirming the complementation and the linkage of the growth defects to the *radA* allele.

Fertility defects of *radA* plants

Arabidopsis *radA* could produce flower stems, but with very small siliques that mainly contained aborted seeds. The few seeds that were produced were heterogeneous in shape and only few germinated (Figure 5A and 5B). To better understand the reduced fertility of *radA* plants we observed both male and female organs. Anthers of *radA* produced pollen that stained positive by Alexander staining, suggesting that it was viable. But microscope inspection of anthers showed that pollen production was reduced compared to WT, and that there was a significant proportion of pollen grains of aberrant size and shape (Figure 5C). Thus, one reason for the partial sterility was low production and low quality of pollen. Regarding female organs, the stigma of *radA* flowers displayed elongated and fully differentiated papillae, but with no attached pollen grains (Figure 5D). Papillae secrete a polysaccharide-rich extracellular matrix optimal for the germination of pollen. Therefore the absence of attached pollen could be because papillae cells were modified and unable to bind pollen. To test whether *radA* female gametes were viable, we backcrossed *radA* with WT pollen, and observed ovules before and after pollination. Flowers from both WT and *radA* were emasculated, and 24h later the mature unfertilized ovules were observed on dissected pistils. The *radA* ovules looked morphologically normal and alike WT ovules, with visible and correctly positioned nuclei of the central and egg cells (Figure 5E left panel). Three days after pollination virtually all WT ovules were fertilized and showed a developing embryo, at the 2 up to 8 cells globular stage. But in *radA* pistils, only 1/6the of the ovules had developing embryos (Figure 5E right panel). The remaining unfertilized ovules either looked normal or were degenerated, with unidentifiable cell types. No elongation of the pollinated pistils was observed. This suggested that normal pollen could not fertilize the apparently normal *radA*

ovules, potentially because of a deficiency in pollen germination in the stigma of *radA* plants. The partial sterility of *radA* would therefore be due to both male and female defects.

radA mutants are affected in the stability of the mitochondrial genome

Several Arabidopsis mutants affected in recombination functions (ex: *msh1, osb1, recA2*, *recA3, recG1*) showed, in normal growth conditions, increased ectopic recombination of the mtDNA across IRs (Gualberto and Newton, 2017). Such events can lead to changes in the stoichiometry of the different regions of the genome, and the severity of the molecular phenotype of increased ectopic recombination normally correlates with the severity of the developmental phenotypes (Arrieta-Montiel et al., 2009; Zaegel et al., 2006). The *radA* mutants were thus also tested for such molecular phenotype. Plants from both *radA-1* and *radA-2* lines of the second homozygous generation were grown *in vitro*. Four of them were selected according to the severity of the visible growth defect phenotype and further analyzed individually (Figure 6A). On these plants the relative copy number of the different mtDNA regions was quantified by qPCR, using a set of primer pairs spaced about 5 kb apart across the genome, as described (Wallet et al., 2015). The recently corrected Arabidopsis Col-0 mtDNA sequence was taken as reference (Sloan et al., 2018). Dramatic changes in the stoichiometry of mtDNA sequences were observed in all plants (Figure 6B). These affected similar regions of the genome in the individual plants, but the amplitude of the changes was higher in the severely affected plants (*radA-1#1* and *radA-2#1*) than in the mildly affected ones (*radA-1#2* and *radA-2#2*). An increase in copy number of large genomic regions could be observed, that could be as high as 7 fold. Several of the observed events of stoichiometry variation corresponded to regions flanked by pairs of directly oriented repeats, including the pair of repeats A (556 bp), F (350 bp), L (249 bp), and EE (127 bp) (Figure 6B). This suggested that the process at play was the same as that described for repeat EE in the *RECG1* KO mutant, *i.e.* the looping out of a circular subgenome by recombination across directly oriented IRs, followed by an autonomous replication (Wallet et al., 2015). We tested by qPCR the accumulation of corresponding crossover products for repeats F, L and EE, as previously described (Miller-Messmer et al., 2012; Wallet et al., 2015). Analysis of recombination involving repeats A was not possible, because the size of the region to be amplified (larger than 600 bp) was not compatible with qPCR. As expected, in all plants a significant increase in crossover products *versus* WT levels was observed for all analyzed repeats (Figure 6C), with a significantly higher accumulation in the more affected plants than in the mildly affected ones. Recombination resulted in the asymmetrical accumulation of mainly one of the two crossover products, with the remarkable exception of recombination involving the pair of repeats L, which resulted in the accumulation of only one of the reciprocal crossover products in mildly affected plants, while both products accumulated in

the severely affected plants. As described before, asymmetric accumulation of only one of the reciprocal recombination products could be because of repair of DSBs by error-prone break-induced replication (BIR), triggered by a deficiency in HR functions required for accurate replication-coupled repair (Gualberto and Newton, 2017; Christensen, 2018). Big differences in the relative accumulation of recombination products were seen, depending on the pair of repeats analyzed. But these values are misleading, because they are compared to the basal levels that exist in WT plants. Thus, a 30 fold increase in recombination product L-1/2 might be equivalent to a 1000 fold increase in product EE-2/1, because the former is already quite abundant in WT Col-0 and easily detected by hybridization, while the latter is virtually absent (Wallet et al., 2015; Zaegel et al., 2006).

Because RADA is also targeted to chloroplasts, the chloroplast DNA (cpDNA) of *radA* plants was likewise scanned for changes in sequence stoichiometry. No changes were detected between mutant and WT, apart from a slight general increase in cpDNA copy number in several individual plants, but below two fold and therefore probably not significant (Supplemental Figure7). Thus, in contrast to the major effects observed on mtDNA maintenance, the loss of RADA apparently does not significantly affect the replication and segregation of the cpDNA in Arabidopsis.

The *radA* mutation is synergistic with *recA3* but not with *recG1*

In bacteria the *radA* mutation is highly synergistic with *recG*. We therefore tested the epistatic relationship between Arabidopsis *RADA* and *RECG1,* in *recG1 radA* double mutants. To compare all mutant plants at the first homozygous generation, heterozygous *recG1-2* plants (KO for *RECG1*, Wallet et al. 2015) were crossed with *radA-1* heterozygous plants used as pollen donor. Double heterozygous (*RECG1+-/RADA+-*) F1 plants were selected, and in the segregating F2 generation we obtained WT, *recG1-2, radA-1* and *recG1-2 radA-1* double homozygous mutants. In this cross, plants inherit the mtDNA of accession Ws, which is the genetic background of *recG1-2.* As described, the *recG1-2* single mutants were similar to WT (Wallet et al., 2015). The *radA-1* single mutants developed the same growth defect phenotypes observed in the Col-0 background. However, the *recG1-2 radA-1* double mutants were as severely affected in growth as *radA-1* plants, with no evidence of a negative epistasis between the two mutations (Figure 7A). Thus, contrarily to bacteria, in plants the *recG1* and *radA* mutations are not synergistic, and RADA contributes to a higher extent to mitochondrial genome maintenance than does RECG1.

It was previously shown that *recG1* is synergistic with mutants deficient for *RECA3* (Wallet et al., 2015), which encodes a RecA ortholog that is dispensable, contrarily to RECA2 (Miller-Messmer et al., 2012). Therefore we also tested the epistatic relationship between *radA* and *recA3.* The *recA3-2* and *radA-1* mutants (both in Col-0 background) were crossed,

using heterozygous plants as female and pollen donor, but no double homozygous mutants could be retrieved from F2 plants growing on soil. Seeds from sesquimutant *RECA3-/- RADA+/-* were germinated *in vitro* and seedlings were genotyped, revealing that double homozygous *recA3 radA1* mutants could germinate, but were unable to grow roots and to further expand their cotyledons (Figure 7B). This seedling lethal phenotype was similar to the one of *recA2* (Miller-Messmer et al., 2012). The synergistic effect of the *radA* and *recA3* mutations suggests that the two factors intervene in alternative pathways, and that compromising both of these leads to a defect equivalent to the loss of the main RECA2-dependent recombination pathway.

The double mutants were tested for their cumulative effects on mtDNA stability. In the genetic background of the Ws mtDNA the effect of the *recG1* KO mutation was mainly the accumulation of the episome resulting from the recombination across the pair of direct repeats EE (Wallet et al., 2015). We tested the accumulation of this episome in *recG1-2,* in *radA-1* and in the double mutant *recG1-2 radA-1* (Figure 7C). In the first homozygous mutant generation we found a mild effect of *recG1-2* on the accumulation of the EE episome, 3 fold more abundant than the flanking mtDNA regions. The *radA*-1 mutation had an equivalent effect, with an increase of about 3.3 fold as compared to the copy number of the flanking regions. However, in *recG1-2 radA-1* there was a significant increase in EE episome accumulation, with roughly a 10 fold higher copy number than the flanking regions. Thus, at the molecular level the double mutation has an additive impact on the correct segregation of mtDNA sequences, although without significant effects on plant development.

Regarding *recA3 radA1*, molecular analysis of a pool of double mutant seedlings showed that mtDNA stability was greatly affected, with an overall reduction in copy number as compared to WT seedlings of the same size, some regions being more than 20 fold reduced or increased as compared to neighboring sequences. Thus, the seedling lethality can be explained by massive problems in the replication and segregation of the mtDNA.

Effects of mtDNA instability on the mitochondrial transcriptome

As discussed above, the instability of the mtDNA in *radA* plants correlated with the severity of the growth defect phenotypes. However, in no case we found a significant reduction in copy number of a gene-containing sequence that could easily correlate the phenotype with a defect in mtDNA gene expression. In order to understand the reason of the *radA* growth defects we quantified by RT-qPCR the relative abundance of most mtDNA-deriving protein gene transcripts and rRNAs. Surprisingly, we found no apparent defects in mtDNA gene expression. For most transcripts we rather observed an increased accumulation as compared to WT plants of the same size (Figure 8A), up to 8-fold in the case of the *rps4* transcript. Because reshuffling of the mtDNA sequences by recombination

can change the expression of non-coding ORFs and even lead to the expression of chimeric genes we also tested the expression of a few mtDNA ORFs whose transcription could be affected by recombination across IRs. These included orf195, a chimera containing the N-terminus of rps3 as a result of recombination across repeats A (Figure 8B), orf315, which is part of a chimera with the N-terminus of atp9 following recombination across repeats G, as well as orf262a and orf255, which might be transcriptionally activated by recombination involving repeats E, L or H. Indeed we found an 8-fold increase in the abundance of orf195 and orf315 transcripts, whose expression is driven by the *rps3* and *atp9* promoters, respectively. Thus, one of the possible reasons for the *radA* growth defects could be the expression of toxic ORFs generated by recombination and that interfere with the synthesis of mitochondrial OXPHOS subunits or with the assembly of OXPHOS complexes.

Instability of the mtDNA in *radA* mutants affects cell cycle progression

Scanning electron microscopy (SEM) showed that *radA* epidermal leaf cells were much enlarged as compared to cells of WT leaves (Figure 9A). The *radA* leaves also had significantly fewer stomata (384.mm^{-2} in *radA-1 versus* 779.mm^{-2} in WT, χ^2 test=8.5E-14). This suggested an inhibition of cell division. To test such a possibility, we measured nuclear DNA ploidy levels by flow cytometry, in the fully developed first true leaves of 20-day-old *radA* and WT plants (Figure 9B and C). We found that *radA* leaves displayed a higher proportion of 4C and 8C nuclei than WT leaves, and an important reduction in 16C nuclei, suggesting that endoreduplication is inhibited in *radA* mutants. In all samples an accumulation of intermediate peaks (ex. 8-16C) was observed in all *radA* samples, but not in WT, also suggesting a blockage of cell cycle progression in S phase, or an induction of programmed cell death. To further explore whether mtDNA instability in *radA* impacts cell cycle progression we quantified nuclear DNA replication, using the thymidine analog 5-ethynyl-2'-deoxyuridine (EdU) to label newly replicated DNA in root tips. In *radA*, the ratio of EdU-positive nuclei was significantly reduced (Figure 9D). Counting of mitotic events in root tips also showed much reduced numbers of cells undergoing mitosis in *radA* (Figure 9E).

It is known that cell cycle checkpoints adjust cellular proliferation to changing growth conditions, arresting it by inhibiting the main cell cycle controllers that include cyclin-dependent kinases (CDKs) (Nowack et al., 2012). In plants, *SMR* genes encode inhibitors of CDK-cyclin complexes that are transcriptionally induced in response to changing conditions, integrating environmental and metabolic signals with cell cycle control (Dubois et al., 2018; Hudik et al., 2014; Yi et al., 2014). Interestingly, chloroplastic defects have been shown to induce cell cycle arrest through the induction of *SMR5* and *SMR7* (Hudik et al., 2014). How these genes are activated remains to be fully elucidated, but the mechanism could involve the activation of the DNA damage response (DDR). This signaling cascade is controlled by

the ATM and ATR kinases (Abraham, 2001) that phosphorylate the SOG1 transcription factor, leading to the up-regulation of thousands of target genes, including *SMR5* and *SMR7* (Yoshiyama, 2016; Yoshiyama et al., 2013). We have therefore tested the expression of several cell cycle markers and of several genes that are transcriptionally activated as part of the DDR. These included 14 *SMR* genes, selected cell cycle-related genes and the NAC-type transcription factors ANAC044 and ANAC085 that inhibit cell cycle progression in response to DNA damage through their activation by SOG1, but also in response to heat stress through a SOG1-independent pathway (Takahashi et al., 2019). Among the 14 SMR genes tested, we found strong induction of *SMR5* in *radA* (Figure 9F, left panel). But transcription of *SMR7*, whose activation has been described as associated with that of *SMR5* in the case of chloroplastic defects (Hudik et al., 2014; Yi et al., 2014), remained unchanged. ANAC085 was also transcriptionally activated in *radA,* more than 30-fold as compared to WT (Figure 9F, right panel). In addition, we observed a low-level, possibly not biologically significant, induction of the DDR genes *BRCA1* and *RAD51*, and of the *CYCB1;1* gene encoding a cyclin associated with G2 arrest and DSB repair (Weimer et al., 2016).

SMR5 is a cyclin-dependent kinase inhibitor that is induced by different conditions leading to oxidative stress (Peres et al., 2007). ROS-dependent transcriptional activation of *SMR5* and of *SMR7* was confirmed in several ROS-inducing conditions (Yi et al., 2014). We have therefore tested whether the induction of *SMR5* in *radA* mutants could be due to the accumulation of ROS. Whole rosettes of WT and *radA* plants of same size were stained with nitro blue tetrazolium (NBT), to reveal for O^{2-}, and a much higher accumulation of ROS was indeed confirmed in *radA* plants (Figure 9F).

Thus, an apparent component of the *radA* phenotype is a retrograde response that activates cell cycle regulators to inhibit cell proliferation. This could be because of the release of ROS from mitochondria, as a consequence of mtDNA instability in the absence of essential HR functions. It is tempting to speculate that the release of ROS results from the accumulation of aberrant proteins that interfere with normal OXPHOS functions.

DISCUSSION

The role of RadA in bacterial HR has been described only very recently (Cooper and Lovett, 2016; Marie et al., 2017). RadA is a hexameric helicase loaded by RecA on either side of the D-loop, to allow hybridization of the invading ssDNA with the recipient DNA (Marie et al., 2017). Our results imply similar functions for plant RADA in organelles, but with a more essential role than that of the bacterial counterpart.

RadA is a RecA paralog, found in all bacteria, algae and land plants. The protein sequence of RadA is well conserved between the various organisms, in particular those of the Walker A, Walker B and KNRFG motifs, as well as the N-terminal zinc finger domain. The modeled structure of plant RADA is very similar to that of *S. pneumoniae* RadA, suggesting that both proteins have the same activities. We established this conservation of activity between plant and bacterial proteins by complementation results and by *in vitro* activity tests. Arabidopsis RADA complements the survival of the bacterial *radA* mutant under genotoxic conditions, as efficiently as the *E. coli* protein when brought in *trans*. Similarly, we show here that plant RADA preferentially binds ssDNA and accelerates the *in vitro* strand-exchange reaction initiated by RecA, as described for bacterial RadA (Cooper and Lovett, 2016). It was previously reported that the rice ortholog is able to promote D-loop formation (Ishibashi et al., 2006). In that report, a different assay system was used, based on the invasion of double-stranded supercoiled plasmid by a labeled oligonucleotide, and the efficiency seemed quite low. With the Arabidopsis recombinant protein and in our test system we could not reproduce such an activity. As reported for bacterial RadA, we found that Arabidopsis RADA is not able to initiate strand invasion, and can only promote branch-migration.

Nevertheless, differences between the activities of Arabidopsis RADA and bacterial RadA were observed. RADA could bind ssDNA-containing molecules without the need for ADP or ATP. But in the presence of ADP or ATP it formed higher molecular weight complexes with ssDNA, suggesting a higher degree of protein oligomerization. In contrast, the presence of ATP activates the translocation of bacterial RadA and causes the dissociation of the protein from DNA (Marie et al., 2017). Only the mutant of the ATPase domain remains associated with DNA in the presence of ATP, because it is unable to activate translocation (Marie et al., 2017). In contrast, both the WT Arabidopsis RADA and the Walker A K201A mutant could bind to ssDNA and form high molecular weight complexes in the presence of ATP or ADP. An explanation would be that under our test conditions the ATPase activity of RADA is not functional, preventing translocation on the DNA. That seems unlikely, given that the recombinant protein could accelerate *in vitro* strand exchange, and should thus have translocase activity. As a whole, the conditions of interaction of RadA (or RADA) with DNA remain controversial. Marie et al. (2017) observed the binding of RadA to

DNA in the absence of ATP, and translocation in the presence of ATP. Cooper and Lovett (2016) observed RadA binding to DNA only in the presence of ADP, while we observed binding of RADA to DNA regardless of the presence of ADP or ATP.

In bacteria, the mutation of a single branch migration factor is only slightly deleterious for cell growth and DNA repair, and that is particularly true for RadA (Beam et al., 2002; Cooper et al., 2015). In plants however, the single loss of RADA severely affects plant development and fertility. This result also contrasts with the lack of a notable developmental phenotype observed for the Arabidopsis *recG1* mutants (Wallet et al., 2015). It therefore seems that in plants RADA has a more important role than RECG1. Since the RuvAB migration pathway is absent in plants, it is possible that HR in plant organelles has evolved by favoring the RADA pathway. Surprisingly, the double mutant *radA recG1* is not more affected in its development than the *radA* single mutant, while in bacteria the mutation of the different branch migration pathways is particularly synergistic (Beam et al., 2002; Cooper et al., 2015). The bacterial *radA recG* double mutant is more severely affected than the *recA* single mutant, indicating that the accumulation of unprocessed branched intermediates is more detrimental to the cell than the lack of recombination. In agreement with this hypothesis, the triple mutant *recA radA recG* is less affected than the *radA recG* double mutant. In plants, the *recA2* mutant is lethal at the seedling stage, and a double mutant *recA2 recA3* could not be segregated, suggesting a more vital role of recombination in organelles than in bacteria (Miller-Messmer et al., 2012). It is therefore surprising that the mutation of all known branch migration pathways in plants is not more deleterious than the mutation of the recombinase.

It is possible that non-processing of recombination intermediates is not as detrimental in plant organelles as in bacteria. But it can also be hypothesized that a further alternative pathway for the processing of recombination intermediates exists in plant organelles. The synergy of the *radA* and *recA3* mutations recalls that observed in the double mutants of bacterial branch migration factors (Cooper et al., 2015). Thus, it might be that RECA3 is involved in the processing of the recombination intermediates created by the RECA2 recombinase, thanks to its branch-migration activity that is intrinsic to RecA-like proteins (Cox, 2007). Furthermore, RECA3 is characterized by the absence of an acidic C-terminal sequence that is found in all other RecA-like proteins, including RECA1 and RECA2 (Miller-Messmer et al., 2012; Shedge et al., 2007). In bacteria, the C-terminus is a site for interaction with many other proteins that regulate RecA activity. Its deletion results in a conformational change in the RecA-DNA filament and enhances almost every one of the RecA functions (Cox, 2007). In eukaryotes, RAD51 paralogs can also be involved in the regulation of recombinase functions (Chun et al., 2013; Qing et al., 2011). As an example, XRCC3, which is part of the CX3 complex, is necessary for the stabilization of

heteroduplexes and controls the extent of gene conversion, thus fulfilling roles reminiscent of branch migration factors (Brenneman et al., 2002). In this respect, RECA3 might have evolved to display enhanced branch migration activity and to be partially redundant to RADA. Nonetheless, unlike RADA, RECA3 apparently retained strand invasion activity, and could partially complement the bacterial *recA* mutant in the repair of UV-induced lesions (Miller-Messmer et al., 2012). RECA3 is therefore also partially redundant with RECA2. Whereas RECA2 and RADA would have specialized in homologous sequence recognition and invasion and branch migration, respectively, RECA3 would be more versatile and have retained both functions.

It is also conceivable that RECA3 acts in an alternative recombination pathway independent of RECA2 and RADA. In the absence of RADA, processing of the intermediates produced by the RECA2 pathway would require activation of the alternative RECA3-dependent recombination pathway. The loss of both RADA and RECA3 would overload the system with unresolved recombination intermediates, which would be lethal for the plant.

We show here that the absence of RADA results in a significant increase in mtDNA ectopic recombination, which leads to drastic changes in the stoichiometry of the genome. These changes are mostly due to the formation of sub-genomes that replicate more rapidly and without coordination with the rest of the mtDNA, as it was observed in the *recG1* mutant for the episome resulting from recombination involving repeats EE (Wallet et al., 2015). The more the stoichiometry of the mtDNA is modified, the more the development of the plant is affected. However, no region of the mtDNA containing functional genes is lost, and all mitochondrial genes that were tested are expressed. The expression of tRNAs has not been tested, but no region comprising a tRNA gene is lost in *radA* plants. Thus, we could not correlate the developmental phenotypes with the reduced expression of a transcript for an OXPHOS subunit, or of a factor required for OXPHOS subunit synthesis and assembly. Nevertheless, the increase in ectopic recombination can lead to the creation and expression of chimeric genes that could encode toxic proteins (Hanson and Bentolila, 2004; Touzet and Meyer, 2014).

Despite dual targeting, the absence of RADA does not seem to affect the chloroplast. As for *recG1* (Wallet et al., 2015), the stoichiometry of the cpDNA is not modified in *radA* mutants. It is possible that RADA does not act in the chloroplast, or that the absence of IRs in the cpDNA of Arabidopsis limits the possibilities of ectopic recombination that could destabilize the genome. RECA2 is also targeted to the chloroplast, but its loss also does not seem to have any deleterious effects in the maintenance of the cpDNA (Miller-Messmer et al., 2012; Shedge et al., 2007).

The cell cycle is an energy demanding process that can be arrested by defects in respiration or photosynthesis (Riou-Khamlichi et al., 2000). Such alterations of organellar

functions can be perceived by the nucleus through retrograde signals leading to a modulation of plant development *via* the control of the cell cycle (Hudik et al., 2014). The severe developmental phenotypes elicited in *radA* mutants indeed seem to partially result from a mitochondrial retrograde signaling that promotes an inhibition of cell cycle progression. That was suggested by the increased size of epidermal cells and the reduction in the number of stomata, and confirmed by determination of nuclear ploidy and incorporation of EdU. The increase of *SMR5* and *ANAC085* transcripts in the *radA* mutants also indicates that the cell cycle is affected by RADA deficiency. SMR5 (with SMR7) is an inhibitor of the cell cycle induced by oxidative, hydric or light stresses (Dubois et al., 2018; Hudik et al., 2014; Yi et al., 2014). These stresses produce ROS that can be retrograde signals to the nucleus (Mittler et al., 2011). Inhibition of the cell cycle can lead to early differentiation of cells causing stunting (Hudik et al., 2014). It is thus possible that mitochondrial genome instability in the *radA* mutants results in sub-optimal function of the OXPHOS complexes and in ROS production, triggering a DNA-damage response, the arrest of the cell cycle and the developmental phenotypes observed.

Since accumulation of ROS has been shown to lead to SOG1 phosphorylation (Yi et al., 2014), the cell cycle inhibition observed in *radA* could result from SOG1-dependent DDR activation. Indeed, DDR mutants, and particularly *sog1,* are hypersensitive to genotoxins targeting organelles (Pedroza-Garcia et al., 2019), supporting the notion that DDR can be activated through retrograde signaling involving ROS production. In line with this hypothesis, expression of the direct SOG1 target *SMR5* was increased in *radA* mutants. However, other SOG1 targets such as *BRCA1* or *CYCB1;1* were only mildly induced in *radA* mutants, suggesting that the SOG1 pathway was not fully activated. Interestingly, the ANAC085 transcription factor, and to a lesser extend ANAC044, which are are known SOG1 targets but have also been shown to respond to abiotic stress independently of SOG1, were induced in *radA*, which could account for the inhibition of cell proliferation. In addition, ANAC044 and ANAC085 are required for the induction of programmed cell death in response to DNA damage (Takahashi et al., 2019). The accumulation of nuclei with intermediate DNA content could thus reflect the induction of cell death in the *radA* mutants. Further work will thus be required to fully decipher how defects in the maintenance of the mitochondrial genome integrity can lead to the inhibition of cell cycle progression.

METHODS

Plant Material:

Arabidopsis T-DNA insertion mutant lines, all in the Col-0 background, were obtained from the Nottingham Arabidopsis Stock Centre (*radA-1*: SALK_097880, *radA-2*: WiscDsLoxHs058_03D). Plant genotypes were determined by PCR using gene and T-DNA specific primers. Seeds were stratified for 3 days at 4 °C and plants were grown on soil or on half-strength MS medium (Duchefa) supplemented with 1 % (w/v) Sucrose, at 22 °C. DNA was extracted using the cetyltrimethylammonium bromide method. RNA was extracted using TRI Reagent (Molecular Research Centre, Inc.). For RT-qPCR experiments, 5 µg of RNA were depleted from contaminating DNA by treatment with RQ1 RNase-free DNase (Promega) and were reverse-transcribed with Superscript IV Reverse Transcriptase (Thermo Fisher Scientific), according to the manufacturer's protocol using random hexamers. For mutant complementation, the WT *RADA* gene and promoter sequence was cloned in binary vector pGWB13, fused to a C-terminal 3xHA tag, and used to transform heterozygous *radA-1* plants. Expression of the transgene in the T1 transformants was monitored by western-blot with a HA-specific antibody.

Bioinformatics analysis

Bacterial and plant sequences were identified in the databases by BLASTP and TBLASTN. Alignments were constructed with ClustalW implemented in the Macvector package using the GonneT matrix. Phylogenetic trees were built with PhyML v3.1 (www.phylogeny. fr) using the neighbor-joining method implemented in the BioNJ program. Graphical representations were performed with TreeDyn (v198.3). The Arabidopsis RADA structure was modeled on the structure of RadA from *Streptococcus pneumoniae* (pdb: 5LKM), using Modeller (http://salilab.org/modeller/about_modeller.html).

Intracellular Localization

The cDNA sequence coding the Arabidopsis RADA N-terminal domain (first 174 codons) was cloned into the pUCAP-GFP vector, derived from pCK-GFP3 (Vermel et al., 2002), and the expressing cassette under control of a double 35S promoter was transferred to the binary vector pBIN+ (van Engelen et al., 1995). Arabidopsis Col-0 plants were transformed by the floral dip method and leaves of selected transformants were observed on a Zeiss LSM700 confocal microscope. The fluorescence of GFP and chlorophyll was observed at 505 to 540 nm and beyond 650 nm, respectively. For mitochondrial co-localization, leafs were infiltrated with a 1/1000 dilution of MitoTraker® orange (Thermo Fisher Scientific) solution. Excitation was at 555 nm and observation at 560-615 nm.

In vitro strand exchange reaction:

Recombination assays were performed with single-strand linear ΦX174 virion DNA and double strand circular ΦX174 RFI DNA (New England Biolabs) linearized with PstI in 20 mM Tris-acetate pH 7.4, 12.5 mM phosphocreatine, 10 U/mL creatine kinase, 3 mM ammonium glutamate, 1 mM dithiothreitol, 2 % glycerol and 11 mM magnesium acetate. In our conditions, 20.1 µM (in nucleotides) linear single strand DNA (ssDNA), 6.7 µM RecA (New England Biolabs), 2 µM RADA are incubated with buffer for 8 min at 37 °C. Then, 20.1 µM (in nucleotides) linear double-strand DNA (dsDNA) is added and the whole reaction is incubated for 5 min at 37 °C. Finally, strand exchange is initiated by adding 3 mM ATP and 3.1 µM SSB (Merck). Aliquots are stopped at indicated times by addition of 12 µM EDTA and 0.8 % SDS. Strand exchange products were analyzed on 0.8 % agarose gels run at 4 °C in Tris-acetate EDTA buffer (TAE) at 50 V and visualized after migration by ethidium bromide staining. For reactions terminated in the absence of RecA, the RecA-initiated strand exchange reaction was stopped at the indicated time and DNA was deproteinized by phenol-chloroform extraction followed by ethanol precipitation. The DNA pellet was solubilized in reaction buffer, 2 µM RADA was added and the reaction was further incubated at 37 °C for the indicated time, before quenching with 12 µM EDTA and 0.8 % SDS.

DNA Binding Assays

For electrophoretic mobility shift assays (EMSA) the purified recombinant protein (50-500 fmol according to the experience) was incubated with oligonucleotide probes (0.01 pmol-10 fmol) that were 5'-radiolabeled with [γ-32P]ATP (5000 Ci/mmol; PerkinElmer Life Science) and T4 polynucleotide kinase (Thermo Fisher Scientific). Different dsDNA structures were prepared by annealing the radiolabeled sense oligonucleotides with a twofold excess of unlabeled complementary oligonucleotide and purified on non-denaturing polyacrylamide gels. The binding reactions were performed in 20 mM Tris-HCl pH 7.5, 50 mM KCl, 5 mM $MgCl_2$, 0.5 mM EDTA, 10 % glycerol, 1 mM DTT and protease inhibitors (Complete-EDTA; Roche Molecular Biochemicals), incubated at 20 °C for 20 min and run on 8 or 4.5 % polyacrylamide gels in Tris-Borate-EDTA buffer at 4 °C. After drying gels were revealed using a Amersham Typhoon phosphorimager (GE Healthcare Life Sciences). For competition assays, labeled probe and unlabeled competitor were added simultaneously to the reaction mixture.

Recombinant proteins

Constructs pET28-RADA and pET28A-RADA[K201A] were used to express recombinant proteins in *E. coli* Rosetta 2 (DE3) pLysS (Novagen). Transformed bacteria were grown at

37 °C until OD_{600nm} = 0.6. Cultures were then chilled to 4 °C for 30 min before addition of 0.5 mM isopropyl b-D-1-thiogalactopyranoside (IPTG) and overnight incubation at 18 °C. After growth cells were pelleted, resuspended in 50 mM Tris-HCl pH 8.0, 5 % glycerol, 300 mM NaCl, 10 mM imidazole, supplemented with 1 mM PMSF and 1 X cOmplete protease inhibitors (Merck) and lysed with a French press under 1200 PSI. The crude lysate was sonicated for 3 min, clarified by 25 min centrifugation at 17700 g and filtrated trough a Filtropur S plus 0.2 µm filter (Sarstedt). The recombinant RADA and RADA[K201A] proteins were affinity purified in a precalibrated HisTrap FF Crude (GE Healthcare Life Sciences) column run at 0.5 mL/min, washed with 50 mM Tris-HCl pH 8.0, 300 mM NaCl, 5 % glycerol, 50 mM imidazole and eluted with a 50-500 mM imidazole gradient. The recombinant protein fractions was further purified by gel filtration on Superdex S200 columns and aliquots were flash frozen in liquid nitrogen and stored at -80 °C. RADA concentration was determined by spectrophotometry using an extinction coefficient of 42,440 M^{-1} cm^{-1}.

Bacterial complementation

The *E. coli* TOP10 strain was used for routine cloning, whereas the BW25113 *radA+* and JW4352 *radA785(del)::kan* were used for complementation assays. The Arabidopsis RADA cDNA (sequence coding for amino acids 137 to 627) or the *E. coli* RadA/Sms sequence were cloned between the PstI and BamHI restriction sites of the pACYCLacZ vector (Miller-Messmer et al. 2012) under the control of the *lac* promoter. Both constructs were introduced in the JW4352 strain. The pACYCLacZ empty vector was introduced in the BW25113 and JW4352 strains as control. Bacteria were grown in LB supplemented with 10 µg/mL chloramphenicol till OD_{600nm} = 0.4 before addition of 2.5 mM IPTG. At OD_{600nm} = 1.2 bacteria were diluted 10^4 fold and grown on LB agar plates supplemented with 15 nM ciprofloxacin, 2 mM IPTG and 10 µg/mL chloramphenicol.

qPCR Analysis

qPCR experiments were performed in a LightCycler480 (Roche) in a total volume of 6 µL containing 0.5 mM of each specific primer and 3µl of SYBR Green I Master Mix (Roche Applied Science). The second derivative maximum method was used to determine Cp values and PCR efficiencies were determined using LinRegPCR software (http://LinRegPCR.nl). Three technical replicates were performed for each experiment. Results of qPCR and RT-qPCR analysis were standardized as previously described (Wallet et al., 2015). Quantification of mtDNA and cpDNA copy numbers used a set of primer pairs located along the organellar genomes, as described previously (Wallet et al. 2015; Le Ret et al. 2018). Results were normalized against the UBQ10 (At4G05320) and ACT1 (At2G37620) nuclear genes. The accumulation of ectopic recombination in mtDNA was quantified using primers

flanking each repeats, as described (Miller-Messmer et al. 2012). The COX2 (AtMG00160) and 18S rRNA (AtMG01390) mitochondrial genes and the 16S rRNA (AtCG00920) chloroplast gene were used for normalization. For RT-qPCR experiments the GAPDH (At1G13440) and ACT2 (At3G18780) transcripts were used as standards.

Flow cytometry and EdU staining

Nuclear DNA content was measured in leaves of 20-d-old seedlings, using the CyStain UV Precise P Kit (Partec) according to the manufacturer's instructions. Nuclei were released in nuclei extraction buffer (Partec) by chopping with a razor blade, stained with 4',6-diamidino-2-phenylindole (DAPI) buffer and filtered through a 30 µM Celltrics mesh (Partec). Between 20,000 and 30,000 isolated nuclei were used for each ploidy level measurement using the Attune Cytometer and the Attune Cytometer software (Life Technologies). At least four independent biological replicates were analyzed. EdU staining was as described (Pedroza-Garcia et al., 2016). For each root tip (n>10), the number of mitotic events was counted directly under the microscope.

Accession Numbers

Sequence data from this article can be found in the Arabidopsis Genome Initiative or GenBank/EMBL databases under the following accession numbers: *RADA*, At5g50340; *RECG1*, At2g01440; *RECA3*, At3g10140; *ANAC044*, At3g01600; *ANAC085*, At5g14490; *KNOLLE*, At1g08560; *CDKB1;2*, At2g38620; *EHD2*, At4g05520; *PLE*, At5g51600; *MYB3R3*, At3g09370; *MYB3R4*, At5g11510; *CYCD3;1*, At4g34160; *CYCD3;2*, At5g67260; *CYCD3;3*, At3g50070; *MCM2*, At1g44900; *MCM3*, At5g46280; *PCNA1*, At1g07370; *PCNA2*, At2g29270; *CDT1a*, At2g31270; *CycB1;1*, At4g37490; *WEE1*, At1g02970; *BRCA1*, At4g21070 ; *RAD51*, At5g20850 ; *XRI1*, At5g48720; *SIM*, At5g04470; *SMR1*, At3g10525; *SMR2*, At1g08180 ; *SMR3*, At5g02420; *SMR4*, At5g02220; *SMR5*, At1g07500; *SMR6*, At5g40460; *SMR7*, At3g27630; *SMR8*, At1g10690; *SMR9*, At1g51355; *SMR10*, At2g28870; *SMR11*, At2g28330; *SMR12*, At2g37610; *SMR13*, At5g59360.

SUPPLEMENTAL DATA FILES

Supplemental Figure 1. Phylogenetic distribution of RADA.

Supplemental Figure 2. Sequences alignment.

Supplemental Figure 3. Effect of the point mutation K201A.

Supplemental Figure 4. Expression, purification and characterization of recombinant RADA.

Supplemental Figure 5. Sequence specificity of RADA binding to ssDNA.

Supplemental Figure 6. Transmission electron microscope (TEM) images.

Supplemental Figure 7. No apparent effect of RADA deficiency on cpDNA stability.

Supplemental Table 1. Oligonucleotides.

Author Contributions

NC, CN, CR, MLR, ME and JMG performed research. NC, CR, MB, AD and JMG designed the research and analyzed data. NC and JMG wrote the paper.

Acknowledgments

We are grateful to Dr. Sandra Noir for help with flow cytometry, and to Dr. Patrice Polard and Dr. Bénédicte Michel for helpful discussions. This work has been published under the framework of the LABEX [ANR-11-LABX-0057_MITOCROSS] and benefits from a funding from the state managed by the French National Research Agency as part of the "Investments for the future" program.

References

Abraham, R.T. (2001). Cell cycle checkpoint signaling through the ATM and ATR kinases. Genes Dev. **15:** 2177-2196.

Arrieta-Montiel, M.P., Shedge, V., Davila, J., Christensen, A.C., and Mackenzie, S.A. (2009). Diversity of the Arabidopsis mitochondrial genome occurs via nuclear-controlled recombination activity. Genetics **183:** 1261-1268.

Backert, S., Lynn Nielsen, B., and Börner, T. (1997). The mystery of the rings: structure and replication of mitochondrial genomes from higher plants. Trends in Plant Science **2:** 477-483.

Beam, C.E., Saveson, C.J., and Lovett, S.T. (2002). Role for radA/sms in recombination intermediate processing in Escherichia coli. J. Bacteriol. **184:** 6836-6844.

Bendich, A.J. (1996). Structural analysis of mitochondrial DNA molecules from fungi and plants using moving pictures and pulsed-field gel electrophoresis. J. Mol. Biol. **255:** 564-588.

Boesch, P., Weber-Lotfi, F., Ibrahim, N., Tarasenko, V., Cosset, A., Paulus, F., Lightowlers, R.N., and Dietrich, A. (2011). DNA repair in organelles: Pathways, organization, regulation, relevance in disease and aging. Biochim. Biophys. Acta **1813:** 186-200.

Brenneman, M.A., Wagener, B.M., Miller, C.A., Allen, C., and Nickoloff, J.A. (2002). XRCC3 controls the fidelity of homologous recombination: roles for XRCC3 in late stages of recombination. Mol. Cell **10:** 387-395.

Budar, F., Touzet, P., and De Paepe, R. (2003). The nucleo-mitochondrial conflict in cytoplasmic male sterilities revisited. Genetica **117:** 3-16.

Christensen, A.C. (2013). Plant mitochondrial genome evolution can be explained by DNA repair mechanisms. Genome Biol. Evol. **5:** 1079-1086.

Christensen, A.C. (2018). Mitochondrial DNA Repair and Genome Evolution. In *Annual Plant Reviews online*, pp. 11-32.

Chun, J., Buechelmaier, E.S., and Powell, S.N. (2013). Rad51 paralog complexes BCDX2 and CX3 act at different stages in the BRCA1-BRCA2-dependent homologous recombination pathway. Mol. Cell. Biol. **33:** 387-395.

Cooper, D.L., Boyle, D.C., and Lovett, S.T. (2015). Genetic analysis of Escherichia coli RadA: functional motifs and genetic interactions. Mol. Microbiol. **95:** 769-779.

Cooper, D.L., and Lovett, S.T. (2016). Recombinational branch migration by the RadA/Sms paralog of RecA in *Escherichia coli.* eLife **5**.

Cox, M.M. (2007). Motoring along with the bacterial RecA protein. Nat. Rev. Mol. Cell Biol. **8:** 127-138.

Dubois, M., Selden, K., Bediee, A., Rolland, G., Baumberger, N., Noir, S., Bach, L., Lamy, G., Granier, C., and Genschik, P. (2018). SIAMESE-RELATED1 Is Regulated Posttranslationally and Participates in Repression of Leaf Growth under Moderate Drought. Plant Physiol. **176:** 2834-2850.

Forget, A.L., and Kowalczykowski, S.C. (2012). Single-molecule imaging of DNA pairing by RecA reveals a three-dimensional homology search. Nature **482:** 423-427.

Fuchs, P., Rugen, N., Carrie, C., Elsasser, M., Finkemeier, I., Giese, J., Hildebrandt, T.M., Kuhn, K., Maurino, V.G., Ruberti, C., Schallenberg-Rudinger, M., Steinbeck, J., Braun, H.P., Eubel, H., Meyer, E.H., Muller-Schussele, S.J., and Schwarzlander, M. (2019). Single organelle function and organization as estimated from Arabidopsis mitochondrial proteomics. Plant J. 10.1111/tpj.14534.

Gualberto, J.M., and Newton, K.J. (2017). Plant Mitochondrial Genomes: Dynamics and Mechanisms of Mutation. Annu Rev Plant Biol **68:** 225-252.

Hanson, M.R., and Bentolila, S. (2004). Interactions of mitochondrial and nuclear genes that affect male gametophyte development. Plant Cell **16 Suppl:** S154-169.

Hudik, E., Yoshioka, Y., Domenichini, S., Bourge, M., Soubigout-Taconnat, L., Mazubert, C., Yi, D., Bujaldon, S., Hayashi, H., De Veylder, L., Bergounioux, C., Benhamed, M., and Raynaud, C. (2014). Chloroplast dysfunction causes multiple defects in cell cycle progression in the Arabidopsis crumpled leaf mutant. Plant Physiol. **166:** 152-167.

Inoue, M., Fukui, K., Fujii, Y., Nakagawa, N., Yano, T., Kuramitsu, S., and Masui, R. (2017). The Lon protease-like domain in the bacterial RecA paralog RadA is required for DNA binding and repair. J. Biol. Chem. **292:** 9801-9814.

Ishibashi, T., Isogai, M., Kiyohara, H., Hosaka, M., Chiku, H., Koga, A., Yamamoto, T., Uchiyama, Y., Mori, Y., Hashimoto, J., Ausio, J., Kimura, S., and Sakaguchi, K. (2006). Higher plant RecA-like protein is homologous to RadA. DNA Repair (Amst.) **5:** 80-88.

Janska, H., Sarria, R., Woloszynska, M., Arrieta-Montiel, M., and Mackenzie, S.A. (1998). Stoichiometric shifts in the common bean mitochondrial genome leading to male sterility and spontaneous reversion to fertility. Plant Cell **10:** 1163-1180.

Manchekar, M., Scissum-Gunn, K., Song, D., Khazi, F., Mclean, S.L., and Nielsen, B.L. (2006). DNA recombination activity in soybean mitochondria. J. Mol. Biol. **356:** 288-299.

Maréchal, A., and Brisson, N. (2010). Recombination and the maintenance of plant organelle genome stability. New Phytologist **186:** 299-317.

884 **Marie, L., Rapisarda, C., Morales, V., Bergé, M., Perry, T., Soulet, A.-L., Gruget, C.,**
885 **Remaut, H., Fronzes, R., and Polard, P.** (2017). Bacterial RadA is a DnaB-type
886 helicase interacting with RecA to promote bidirectional D-loop extension. Nat.
887 Commun. **8:** 15638.
888 **Miller-Messmer, M., Kuhn, K., Bichara, M., Le Ret, M., Imbault, P., and Gualberto, J.M.**
889 (2012). RecA-dependent DNA repair results in increased heteroplasmy of the
890 Arabidopsis mitochondrial genome. Plant Physiol. **159:** 211-226.
891 **Mittler, R., Vanderauwera, S., Suzuki, N., Miller, G., Tognetti, V.B., Vandepoele, K.,**
892 **Gollery, M., Shulaev, V., and Van Breusegem, F.** (2011). ROS signaling: the new
893 wave? Trends Plant Sci. **16:** 300-309.
894 **Mower, J.P., Touzet, P., Gummow, J.S., Delph, L.F., and Palmer, J.D.** (2007). Extensive
895 variation in synonymous substitution rates in mitochondrial genes of seed plants.
896 BMC Evol. Biol. **7:** 135.
897 **Nowack, M.K., Harashima, H., Dissmeyer, N., Zhao, X., Bouyer, D., Weimer, A.K., De**
898 **Winter, F., Yang, F., and Schnittger, A.** (2012). Genetic framework of cyclin-
899 dependent kinase function in Arabidopsis. Dev. Cell **22:** 1030-1040.
900 **Odahara, M., Masuda, Y., Sato, M., Wakazaki, M., Harada, C., Toyooka, K., and Sekine,**
901 **Y.** (2015). RECG maintains plastid and mitochondrial genome stability by
902 suppressing extensive recombination between short dispersed repeats. PLoS Genet.
903 **11:** e1005080.
904 **Pedroza-Garcia, J.A., Domenichini, S., Mazubert, C., Bourge, M., White, C., Hudik, E.,**
905 **Bounon, R., Tariq, Z., Delannoy, E., Del Olmo, I., Pineiro, M., Jarillo, J.A.,**
906 **Bergounioux, C., Benhamed, M., and Raynaud, C.** (2016). Role of the Polymerase
907 sub-unit DPB2 in DNA replication, cell cycle regulation and DNA damage response in
908 Arabidopsis. Nucleic Acids Res. **44:** 7251-7266.
909 **Pedroza-Garcia, J.A., Najera-Martinez, M., Mazubert, C., Aguilera-Alvarado, P., Drouin-**
910 **Wahbi, J., Sanchez-Nieto, S., Gualberto, J.M., Raynaud, C., and Plasencia, J.**
911 (2019). Role of pyrimidine salvage pathway in the maintenance of organellar and
912 nuclear genome integrity. Plant J. **97:** 430-446.
913 **Peres, A., Churchman, M.L., Hariharan, S., Himanen, K., Verkest, A., Vandepoele, K.,**
914 **Magyar, Z., Hatzfeld, Y., Van Der Schueren, E., Beemster, G.T., Frankard, V.,**
915 **Larkin, J.C., Inze, D., and De Veylder, L.** (2007). Novel plant-specific cyclin-
916 dependent kinase inhibitors induced by biotic and abiotic stresses. J. Biol. Chem.
917 **282:** 25588-25596.
918 **Qing, Y., Yamazoe, M., Hirota, K., Dejsuphong, D., Sakai, W., Yamamoto, K.N., Bishop,**
919 **D.K., Wu, X., and Takeda, S.** (2011). The epistatic relationship between BRCA2 and
920 the other RAD51 mediators in homologous recombination. PLoS Genet. **7:** e1002148.

Ragunathan, K., Liu, C., and Ha, T. (2012). RecA filament sliding on DNA facilitates homology search. eLife **1:** e00067.

Riou-Khamlichi, C., Menges, M., Healy, J.M., and Murray, J.A. (2000). Sugar control of the plant cell cycle: differential regulation of Arabidopsis D-type cyclin gene expression. Mol. Cell. Biol. **20:** 4513-4521.

Shedge, V., Arrieta-Montiel, M., Christensen, A.C., and Mackenzie, S.A. (2007). Plant mitochondrial recombination surveillance requires unusual RecA and MutS homologs. Plant Cell **19:** 1251-1264.

Sloan, D.B. (2013). One ring to rule them all? Genome sequencing provides new insights into the 'master circle' model of plant mitochondrial DNA structure. New Phytologist **200:** 978-985.

Sloan, D.B., Wu, Z., and Sharbrough, J. (2018). Correction of Persistent Errors in Arabidopsis Reference Mitochondrial Genomes. Plant Cell **30:** 525-527.

Small, I., Suffolk, R., and Leaver, C.J. (1989). Evolution of plant mitochondrial genomes via substoichiometric intermediates. Cell **58:** 69-76.

Takahashi, N., Ogita, N., Takahashi, T., Taniguchi, S., Tanaka, M., Seki, M., and Umeda, M. (2019). A regulatory module controlling stress-induced cell cycle arrest in Arabidopsis. eLife **8**.

Touzet, P., and Meyer, E.H. (2014). Cytoplasmic male sterility and mitochondrial metabolism in plants. Mitochondrion **19 Pt B:** 166-171.

Vermel, M., Guermann, B., Delage, L., Grienenberger, J.M., Marechal-Drouard, L., and Gualberto, J.M. (2002). A family of RRM-type RNA-binding proteins specific to plant mitochondria. Proc. Natl. Acad. Sci. U. S. A. **99:** 5866-5871.

Vitart, V., Depaepe, R., Mathieu, C., Chetrit, P., and Vedel, F. (1992). Amplification of substoichiometric recombinant mitochondrial DNA sequences in a nuclear, male sterile mutant regenerated from protoplast culture in Nicotiana sylvestris. Mol. Gen. Genet. **233:** 193-200.

Wallet, C., Le Ret, M., Bergdoll, M., Bichara, M., Dietrich, A., and Gualberto, J.M. (2015). The RECG1 DNA Translocase Is a Key Factor in Recombination Surveillance, Repair, and Segregation of the Mitochondrial DNA in Arabidopsis. Plant Cell **27:** 2907-2925.

Weimer, A.K., Biedermann, S., Harashima, H., Roodbarkelari, F., Takahashi, N., Foreman, J., Guan, Y., Pochon, G., Heese, M., Van Damme, D., Sugimoto, K., Koncz, C., Doerner, P., Umeda, M., and Schnittger, A. (2016). The plant-specific CDKB1-CYCB1 complex mediates homologous recombination repair in Arabidopsis. EMBO J. **35:** 2068-2086.

957 **West, S.C.** (1997). Processing of recombination intermediates by the RuvABC proteins.
958 Annu. Rev. Genet. **31:** 213-244.
959 **Whitby, M.C., Vincent, S.D., and Lloyd, R.G.** (1994). Branch migration of Holliday
960 junctions: identification of RecG protein as a junction specific DNA helicase. EMBO J.
961 **13:** 5220-5228.
962 **Woloszynska, M., and Trojanowski, D.** (2009). Counting mtDNA molecules in Phaseolus
963 vulgaris: sublimons are constantly produced by recombination via short repeats and
964 undergo rigorous selection during substoichiometric shifting. Plant Mol. Biol. **70:** 511-
965 521.
966 **Xu, Y.Z., Santamaria Rde, L., Virdi, K.S., Arrieta-Montiel, M.P., Razvi, F., Li, S., Ren, G.,**
967 **Yu, B., Alexander, D., Guo, L., Feng, X., Dweikat, I.M., Clemente, T.E., and**
968 **Mackenzie, S.A.** (2012). The chloroplast triggers developmental reprogramming
969 when mutS HOMOLOG1 is suppressed in plants. Plant Physiol. **159:** 710-720.
970 **Yi, D., Alvim Kamei, C.L., Cools, T., Vanderauwera, S., Takahashi, N., Okushima, Y.,**
971 **Eekhout, T., Yoshiyama, K.O., Larkin, J., Van Den Daele, H., Conklin, P., Britt,**
972 **A., Umeda, M., and De Veylder, L.** (2014). The Arabidopsis SIAMESE-RELATED
973 cyclin-dependent kinase inhibitors SMR5 and SMR7 regulate the DNA damage
974 checkpoint in response to reactive oxygen species. Plant Cell **26:** 296-309.
975 **Yoshiyama, K.O., Kobayashi, J., Ogita, N., Ueda, M., Kimura, S., Maki, H., and Umeda,**
976 **M.** (2013). ATM-mediated phosphorylation of SOG1 is essential for the DNA damage
977 response in Arabidopsis. EMBO Rep. **14:** 817-822.
978 **Yoshiyama, K.O.** (2016). SOG1: a master regulator of the DNA damage response in plants.
979 Genes Genet. Syst. **90:** 209-216.
980 **Zaegel, V., Guermann, B., Le Ret, M., Andres, C., Meyer, D., Erhardt, M., Canaday, J.,**
981 **Gualberto, J.M., and Imbault, P.** (2006). The plant-specific ssDNA binding protein
982 OSB1 is involved in the stoichiometric transmission of mitochondrial DNA in
983 Arabidopsis. Plant Cell **18:** 3548-3563.
984
985

FIGURE LEGENDS

Figure 1. Arabidopsis RADA is targeted to both chloroplasts and mitochondria.

The RADA:GFP fusion protein was constitutively expressed in transgenic plants and its location observed in leaf epidermal cells. It co-localized with both chloroplasts (autofluorescence of chlorophyll) mitochondria (red fluorescence of MitoTracker).

Figure 2. The Arabidopsis RADA is structurally and functionally homologous to bacterial RadA.

(**A**) The modular structure of plant RADA is similar to the one from bacteria, with a N-terminal zinc-finger (C4), an helicase and Lon-protease-like domains (H and P domains respectively). Plant precursor proteins have an N-terminal extension containing an organellar targeting sequence (OTS). (**B**) Model of Arabidopsis RADA superposed on the known structure of *S. pneumoniae* (in gray) (Marie et al., 2017). The color code of relevant domains is as in A). A bound ADP and the Mg^{2+} ion (yellow ball) are shown. (**C**) Complementation of an *E. coli radA* mutant (ΔRadA) for growth in the presence of genotoxic ciprofloxacin (CIP). Arabidopsis *RADA* (*At*-RADA) complements the mutation as efficiently as the bacterial one (*Ec*-RadA) cloned in the same expression vector.

Figure 3. DNA-binding and branch-migration activities of RADA.

(**A**) EMSA experiments showing that RADA binds any ssDNA-containing DNA structure with higher affinity than dsDNA. Lower and higher molecular weigh complexes are indicated by white and black arrowheads respectively (**B**) Analysis on low concentration gel (4.5 % as compared to 8 % in A) of the formation of a high-molecular weight RADA filament on ssDNA, which is promoted by ATP or ADP (1 mM). The K201A mutant protein binds with equivalent affinity as the WT protein. Increasing concentrations of RADA used in A and B are indicated by the grey triangles. (**C**) In a *in vitro* strand-invasion reaction plant RADA accelerates branch-migration of DNA heteroduplexes initiated by RecA. An explanation of the different substrates and products is shown below the gel. (**D**) Ratio of final product as compared to the initial linear dsDNA substrate in 6 independent experiments, showing that in the presence of RADA there is faster resolution of branched intermediates. (**E**) RADA can alone finalize branch-migration initiated by RecA: a reaction at T=7 min was arrested by deproteination (left panel) and the DNA purified. Without addition of RecA or RADA there is no spontaneous progression of the reaction (middle panel), but RADA alone can resolve intermediates into the final product (right panel). (**F**) RADA alone cannot initiate strand invasion. (**G**) Mutation of the ATPase Walker domain of RADA (K201A) inhibits the reaction.

Figure 4. Arabidopsis *radA* mutants and phenotypes.

(**A**) Schematic representation of the Arabidopsis *RADA* gene. Coding sequences are in black and 5'- and 3'-UTRs are in gray. The position of the T-DNA insertions in *radA* mutant lines is shown. (**B**) *radA* plants show severe growth retardation, with distorted leaves presenting chlorotic sector. These can be complemented by expression of HA-tagged RADA (RADA:HA) under control of the endogenous promoter. (**C**) root shortening of *radA* plants. (**D**) Detail of leaves phenotype. (**E**) Perennial vegetative growth of plants grown on short days (8h light), with development of aerial rosettes (4-month old *radA-1* plant).

Figure 5. Reduced fertility of *radA* plants.

(**A**) Comparison of WT and *radA* flower stems showing very small *radA* siliques. (**B**) *radA* siliques have mostly aborted seeds, and the few seeds produced are mostly non-viable. (**C**) Alexander staining of pollen in *radA* anthers as compared to WT, showing little pollen production, and an abundance of small and aberrant pollen grains (indicated by arrows). (**D**) Visible and SEM Images showing that no pollen binds to the papillae in *radA* stigma. (**E**) Differential interference contrast images of ovules on crosses between *radA-1* flowers and WT pollen. Black arrowheads indicate central cell and egg cell nuclei in unfertilized ovules. White arrowheads indicate developing embryos in fertilized ovules, three days after pollination (DAP). Only 16 % of *radA* ovules could be fertilized. Scale bar is 50 µm. (**F**) After seven DAP the pollinated pistils of *radA* did not develop further.

Figure 6. Changes in mtDNA sequences stoichiometry in *radA* mutants because of increased ectopic recombination across repeats.

(**A**) Picture of severely affected (*radA-1*#1 and *radA-2*#1) and mildly affected (*radA-1*#2 and *radA-2*#2) seedlings that were analyzed. (**B**) Scanning of their mtDNA for changes in relative copy numbers of the different mtDNA regions. Sequences spaced 5-10 kb apart on the mtDNA were quantified by qPCR. Coordinates are those of the Col-0 mtDNA sequence. The position of the mtDNA large repeats LR1 and LR2 and of relevant intermediate size repeats are shown below the graphic. Regions with changed stoichiometries flanked by repeat pairs are shadowed. Error bars are the *SD* values from three technical replicates. (**C**) Accumulation of crossover products from mtDNA repeats L, F and EE in the *radA* seedlings relative to WT. Results are in a log2 scale. The scheme shows the qPCR relative quantification of parental sequences 1/1 and 2/2 and of the corresponding crossover products 1/2 and 2/1. Results are the mean of three technical replicates, and error bars correspond to *SD* values.

Figure 7. Synergistic effects of the *radA* mutation on *recG1* and *recA3*.

(**A**) Crosses of *recG1-2* and *radA-1* (pollen donor) show that double homozygote *recG1 radA* plants are as affected as simple homozygote *radA* plants. (**B**) Crosses and segregation of *recA3-2* and *radA-1* (pollen donor) show that double homozygote *recA3 radA* seedlings do not grow roots and do not grow further. The phenotype is similar to the one observed for *recA2* mutants (Miller-Messmer et al. 2012). The scale bar is 1 mm. (**C**) qPCR analysis of the copy number of mtDNA sequences around and within the region comprised between pair of repeats EE, previously shown to generate an episome by recombination in *recG1* plants (Wallet et al. 2015). Autonomous replication of the episome is significantly increased in the *recG1 radA* double mutant. Results show the mean and SD error bars from 2 or 3 (for *recG1 radA*) biological replicates. (**D**) Scanning of the copy numbers of the different mtDNA regions in *recA3 radA*, as described in Figure 6, showing severe reduction of several mtDNA regions. Results were compared to those of WT seedling of same size, and are in log scale.

Figure 8. Accumulation of mitochondrial transcripts in *radA*.

(A) Representative mitochondrial transcripts were quantified by RT-qPCR, from the RNA of 10-day old seedlings grown *in vitro,* and normalized against a set of nuclear housekeeping genes. The quantification of several transcripts of orfs whose transcription could be potentially affected by ectopic recombination involving IRs are shown on the right, in red. Results are on a log2 scale and are the mean from four biological replicates (two pools of *radA-1* and two pools of *rad-2* seedlings) and corresponding SD error bars. **(B)** Chimeric *orf195* and *orf315* created by recombination whose transcription is augmented in *radA* plants. The regions corresponding to *rps3* and *atp9* sequences are shown in blue. Repeated sequences are represented by orange bars. Coordinates on the mtDNA are indicated.

Figure 9. Cell cycle progression is impaired in *radA* plants.

(A) Scanning electron microscopy images showing that in *radA* leaves epidermal cells are much larger and there are fewer stomata, half the number for the same leaf surface. Scale bar is 20 µm. **(B)** Flow-cytometry profile obtained in WT (Col-0) and *radA.* The DNA content of nuclei extracted from the first true leafs of 20 day-old plants was analyzed. **(C)** Ploidy distribution, showing decreased endoreduplication in the mutant, with an increased proportion of 4C and 8C nuclei and a decreased proportion of 16C nuclei. Values are the average ± SD of 4 experiments for WT and six experiments for *radA* (n>20 000 nuclei). **(D)** Decreased DNA synthesis in the nuclei of *radA* root tip cells, as evaluated by the ratio between EdU positive and DAPI (4',6'-diamidino-2-phénylindol) positive cells. **(E)** Decreased number of cells undergoing mitosis. Significances were calculated by Student's t test. **(F)** RT-qPCR analysis of the expression of a set of cell cycle related genes in 10-day old WT and

radA seedlings, revealing activation of *SMR5* and *ANAC085*. Data is represented in a log2 scale and is the mean ± SE of three biological replicates (two pools of seedlings from *radA-1* and one from *radA-2*). **(G)** NBT (nitro blue tetrazolium) staining for O^{2-} of plants of equivalent size grown under same conditions, showing that *radA* mutants accumulate much more ROS than WT plants. Scale bar is 1 cm.

Supplemental Figure 1. Phylogenetic distribution of RADA.

Genes coding for RadA-like proteins are found in all bacteria, in land plants, green, brown and red algae, diatoms and other organisms of the Stramenopile group. *Arabidopsis thaliana,* NP_199845; *Populus trichocarpa,* EEE84551; *Vitis vinifera,* XP_002277638; *Oryza sativa,* NP_001056828; *Zea mays,* NP_001170708; *Selaginella moellendorffii,* XP_002976563; *Physcomitrella patens,* XP_001757578; *Ostreococcus tauri,* XP_003084463; *Coccomyxa subellipsoidea,* XP_005643141; *Chlorella variabilis,* EFN56488; *Cyanidioschyzon merolae,* XP_005536634; *Galdieria sulphuraria,* XP_005709405; *Ectocarpus siliculosus,* CBJ25917; *Phaeodactylum tricornutum,* XP_002178713; *Thalassiosira oceanica,* EJK58798; *Saprolegnia diclina,* EQC30001; *Phytophthora infestans,* XP_002904225; *Myxococcus xanthus,* YP_629513; *Rickettsia prowazekii,* WP_014607237; *Neisseria meningitidis,* WP_002258526; *Escherichia coli,* WP_001458566; *Microcystis aeruginosa,* WP_002742386; *Synechocystis sp,* WP_009633429; *Geminocystis herdmanii,* WP_017296205; *Bacillus anthracis,* NP_842650; *Amphibacillus jilinensis,* WP_017473696.

Supplemental Figure 2. Sequences alignment.

Sequence alignment (Clustal W) between representative land plant RADA sequences and RadA from proteobacteria and cyanobacteria. The Zinc-finger and KNRFG RadA-specific motif are shaded in yellow and blue respectively, and the Walker A and B motifs in green.

Supplemental Figure 3. Effect of the point mutation K201A.

Effect of the point mutation K201A (amino acids in green) on the Walker A domain of RadA in the binding and hydrolysis of ATP. The structure shown is the one from bacterial RadA (Marie et al. 2017), with bound ADP and Mg^{2+} ion (sphere). The two phosphate groups of ADP are in red.

Supplemental Figure 4. Expression, purification and characterization of recombinant RADA.

The Arabidopsis RADA sequence minus the first 48 codons corresponding to the OTS was cloned in the expression vector pET28a fused to a N-terminal His-tag. The recombinant RADA and Walker mutant K201A were expressed in the Rosetta(DE3) strain and purified by affinity and gel filtration. (**A**) Coomassie gel staining analysis of the recombinant proteins. (**B**) Gel filtration on Superdex S200 showed that RADA purified as two peaks of high molecular weight. (**C**) Dynamic light scattering of the protein fraction from peak 2 shows that it is monodispersed and corresponding to a size of about 340 kDa, which is consistent with an hexameric RADA molecule. (**D**) EMSA analysis of the binding to a ssDNA oligonucleotide.

Fractions corresponding to both peaks give complexes of the same size, although fractions of peak 1 give predominantly higher molecular weight complexes.

Supplemental Figure 5. Sequence specificity of RADA binding to ssDNA.
A 30-mer ssDNA oligonucleotide (7x[AGTC]AG) was used as probe in EMSA experiments with recombinant RADA, and sequence specificity was tested by competition with increasing concentrations of the cold homologous oligonucleotide or with 30-oligomers (poly-A, pol-T, poly-C and poly-G). Competitor/probe ratios tested were 0; 2.5; 10 and 40. Only poly-A showed reduced competition for RADA binding.

Supplemental Figure 6. Transmission electron microscope (TEM) images
TEM images of cells from leaves of same size showed morphologically normal chloroplasts (cp) in *radA.* Mitochondria (mt) were enlarged and less electron dense as compared to mitochondria from WT cells.

Supplemental Figure 7. No apparent effect of RADA deficiency on cpDNA stability.
Scanning of the cpDNA of *radA* mutants for changes in relative copy numbers of the different cpDNA regions. Sequences spaced 5-10 kb apart on the cpDNA were quantified by qPCR, as described for the mtDNA in Figure 6. Values are the mean ± SD of three technical replicates. Coordinates correspond to the ones of the published Col-0 cpDNA sequence. The three major regions of the cpDNA are indicated: LSC, large single copy region; SSC, small single-copy region; IR, inverted repeat.

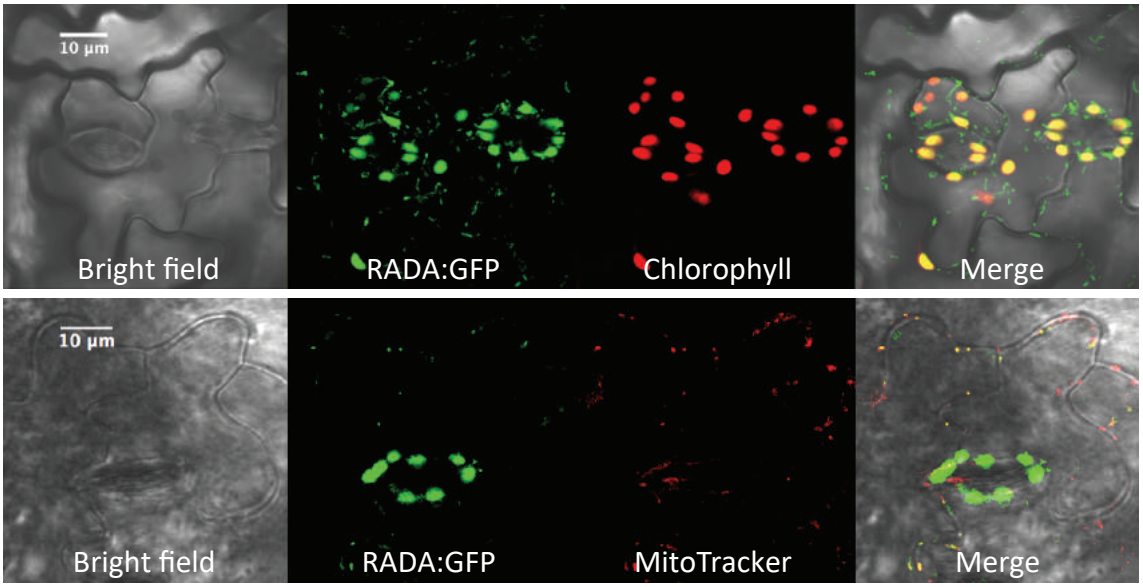

Figure 1. Arabidopsis RADA is targeted to both chloroplasts and mitochondria.
The RADA:GFP fusion protein was constitutively expressed in transgenic plants and its location observed in leaf epidermal cells. It co-localized with both chloroplasts (autofluorescence of chlorophyll) and mitochondria (red fluorescence of MitoTracker).

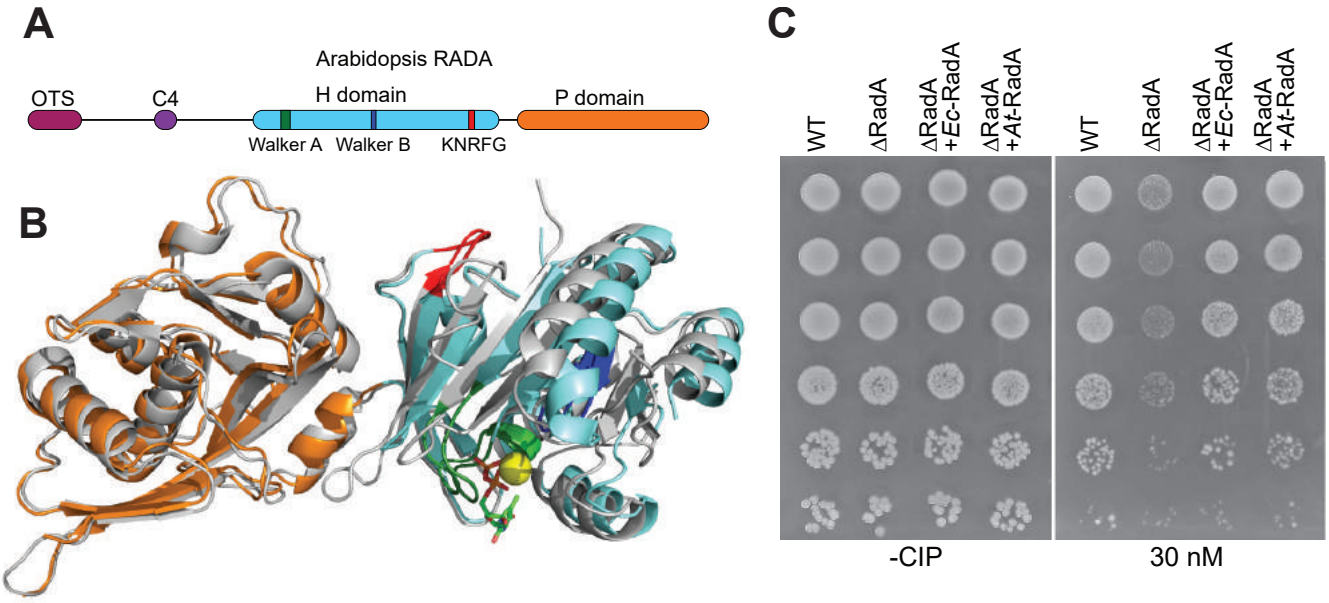

Figure 2. The Arabidopsis RADA is structurally and functionally homologous to bacterial RadA.

(**A**) The modular structure of plant RADA is similar to the one from bacteria, with a N-terminal zinc-finger (C4), an helicase and Lon-protease-like domains (H and P domains respectively). Plant precursor proteins have an N-terminal extension containing an organellar targeting sequence (OTS). (**B**) Model of Arabidopsis RADA superposed on the known structure of *S. pneumoniae* (in gray) (Marie et al., 2017). The color code of relevant domains is as in (A). Bound ADP and the Mg^{2+} ion (yellow ball) are shown. (**C**) Complementation of an *E. coli radA* mutant (ΔRadA) for growth in the presence of genotoxic ciprofloxacin (CIP). Arabidopsis *RADA* (*At*-RADA) complements the mutation as efficiently as the bacterial one (*Ec*-RadA) cloned in the same expression vector.

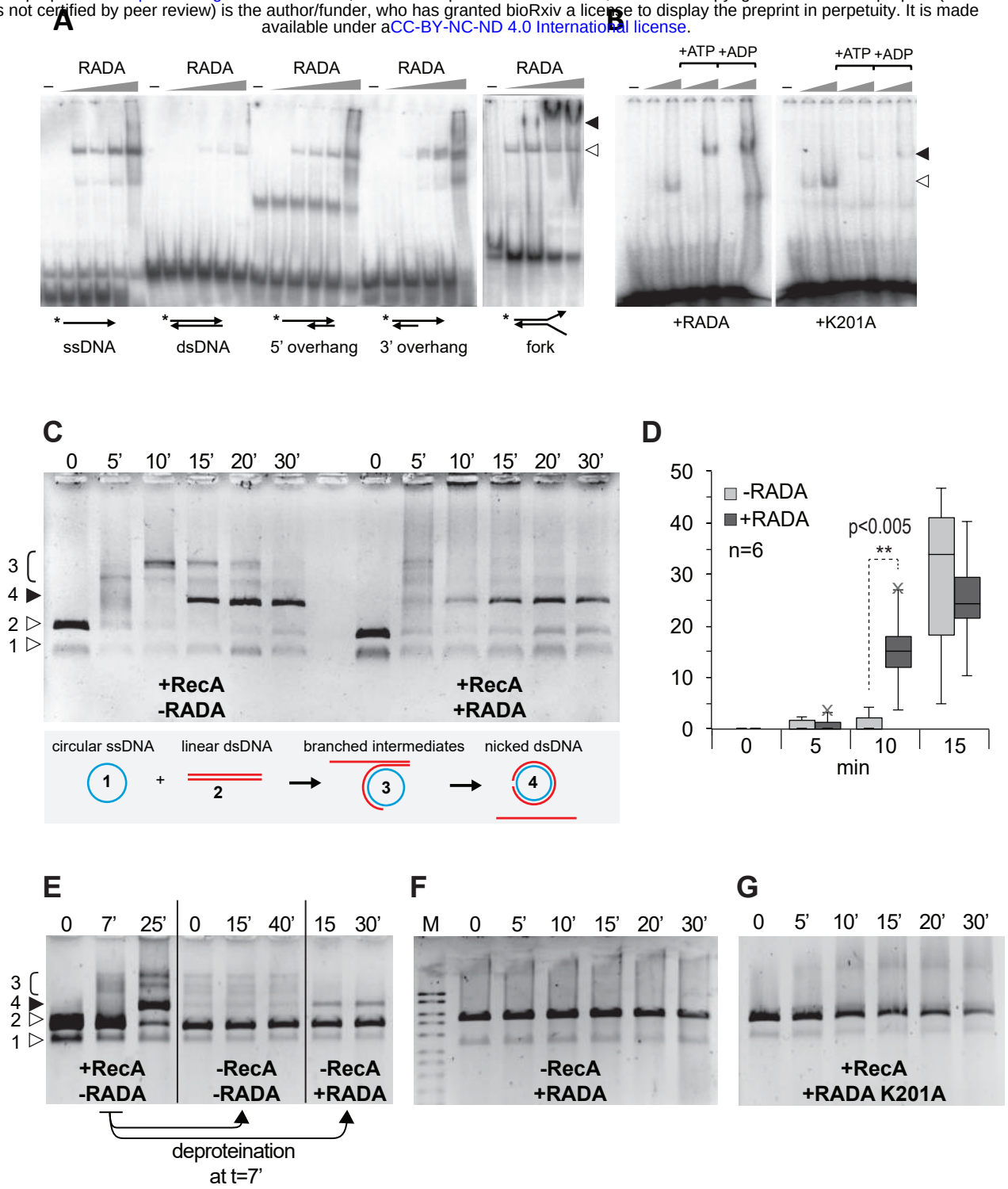

Figure 3. DNA-binding and branch-migration activities of RADA.

(**A**) EMSA experiments showing that RADA binds any ssDNA-containing DNA structure with higher affinity than dsDNA. Lower and higher molecular weigh complexes are indicated by white and black arrowheads respectively (**B**) Analysis on low concentration gel (4.5 % as compared to 6 % in A) of the formation of a high-molecular weight RADA filament on ssDNA, which is promoted by ATP or ADP (1 mM). The K201A mutant protein binds with equivalent affinity as the WT protein. Increasing concentrations of RADA used in A and B are indicated by the grey triangles. (**C**) In a *in vitro* strand-invasion reaction plant RADA accelerates branch-migration of DNA heteroduplexes initiated by RecA. An explanation of the different substrates and products is shown below the gel. (**D**) Ratio of final product as compared to the initial linear dsDNA substrate in 6 independent experiments, showing that in the presence of RADA there is faster resolution of branched intermediates. (**E**) RADA can alone finalize branch-migration initiated by RecA: a reaction at T=7 min was arrested by deproteination (left panel) and the DNA purified. Without addition of RecA or RADA there is no spontaneous progression of the reaction (middle panel), but RADA alone can resolve intermediates into the final product (right panel). (**F**) RADA alone cannot initiate strand invasion. (**G**) Mutation of the ATPase Walker domain of RADA (K201A) inhibits the reaction.

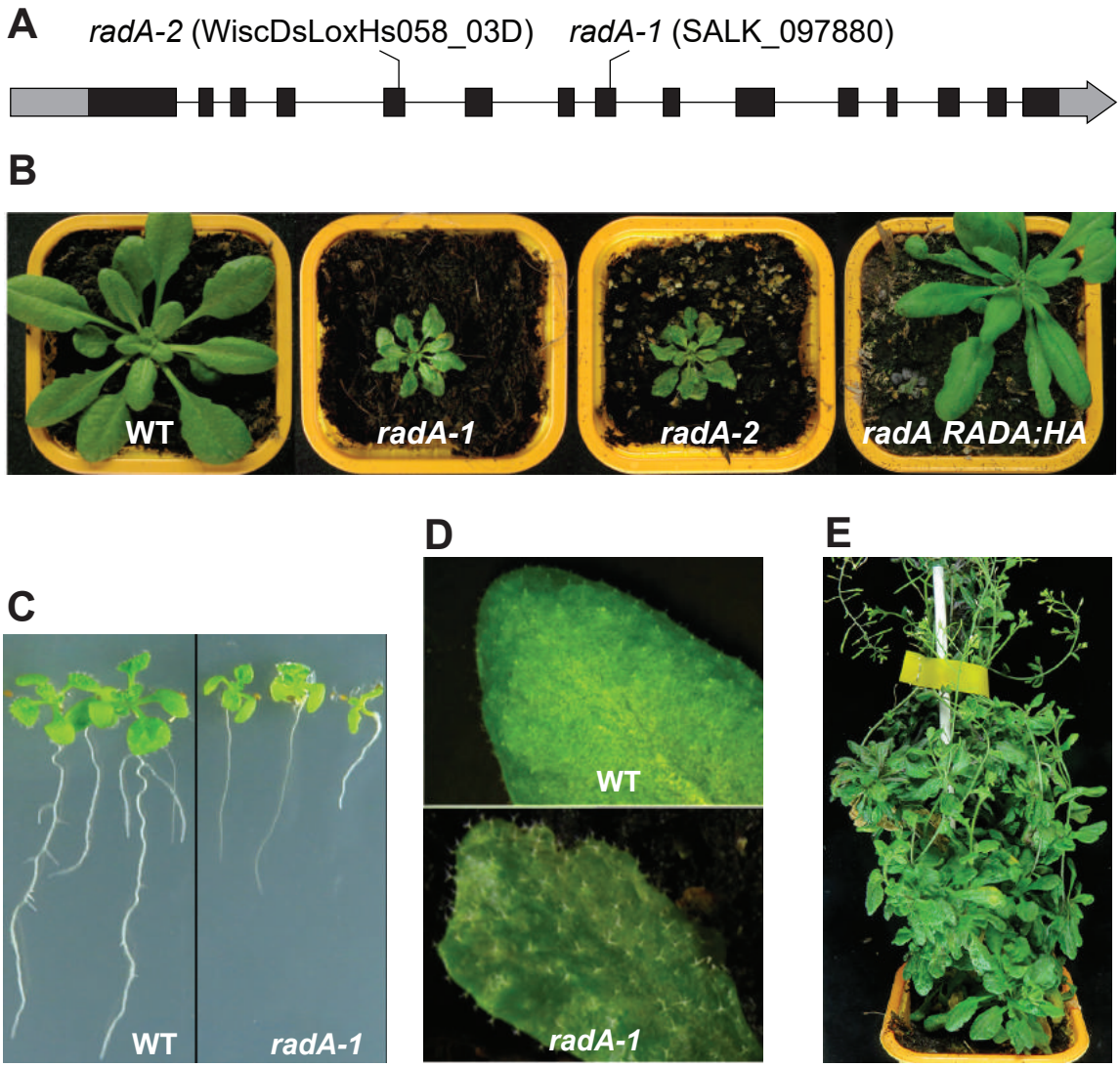

Figure 4. Arabidopsis *radA* mutants and phenotypes.
(**A**) Schematic representation of the Arabidopsis *RADA* gene. Coding sequences are in black and 5'- and 3'-UTRs are in gray. The position of the T-DNA insertions in *radA* mutant lines is shown. (**B**) *radA* plants show severe growth retardation, with distorted leaves presenting chlorotic sector. These can be complemented by expression of HA-tagged RADA (RADA:HA) under control of the endogenous promoter. (**C**) root shortening of *radA* plants. (**D**) Detail of leaves phenotype. (**E**) Perennial vegetative growth of plants grown on short days (8h light), with development of aerial rosettes (4-month old *radA-1* plant).

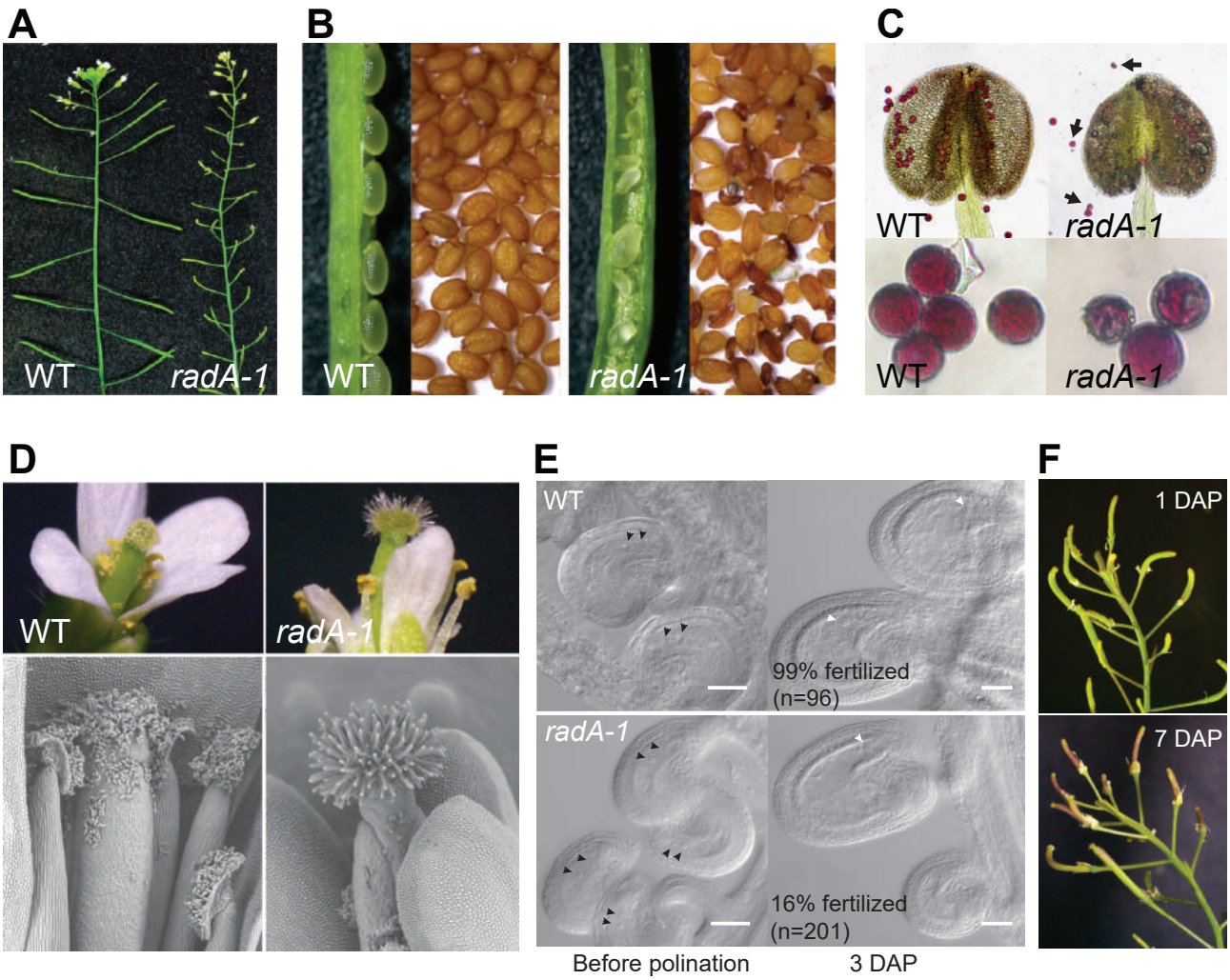

Figure 5. Reduced fertility of *radA* plants.

(**A**) Comparison of WT and *radA* flower stems showing very small *radA* siliques. (**B**) *radA* siliques have mostly aborted seeds, and the few seeds produced are mostly non-viable. (**C**) Alexander staining of pollen in *radA* anthers as compared to WT, showing little pollen production, and an abundance of small and aberrant pollen grains (indicated by arrows). (**D**) Visible and SEM Images showing that no pollen binds to the papillae in *radA* stigma. (**E**) Differential interference contrast images of ovules on crosses between *radA-1* flowers and WT pollen. Black arrowheads indicate central cell and egg cell nuclei in unfertilized ovules. White arrowheads indicate developing embryos in fertilized ovules, three days after pollination (DAP). Only 16 % of *radA* ovules could be fertilized. Scale bar is 50 µm. (**F**)After seven DAP the pollinated pistils of *radA* did not develop further.

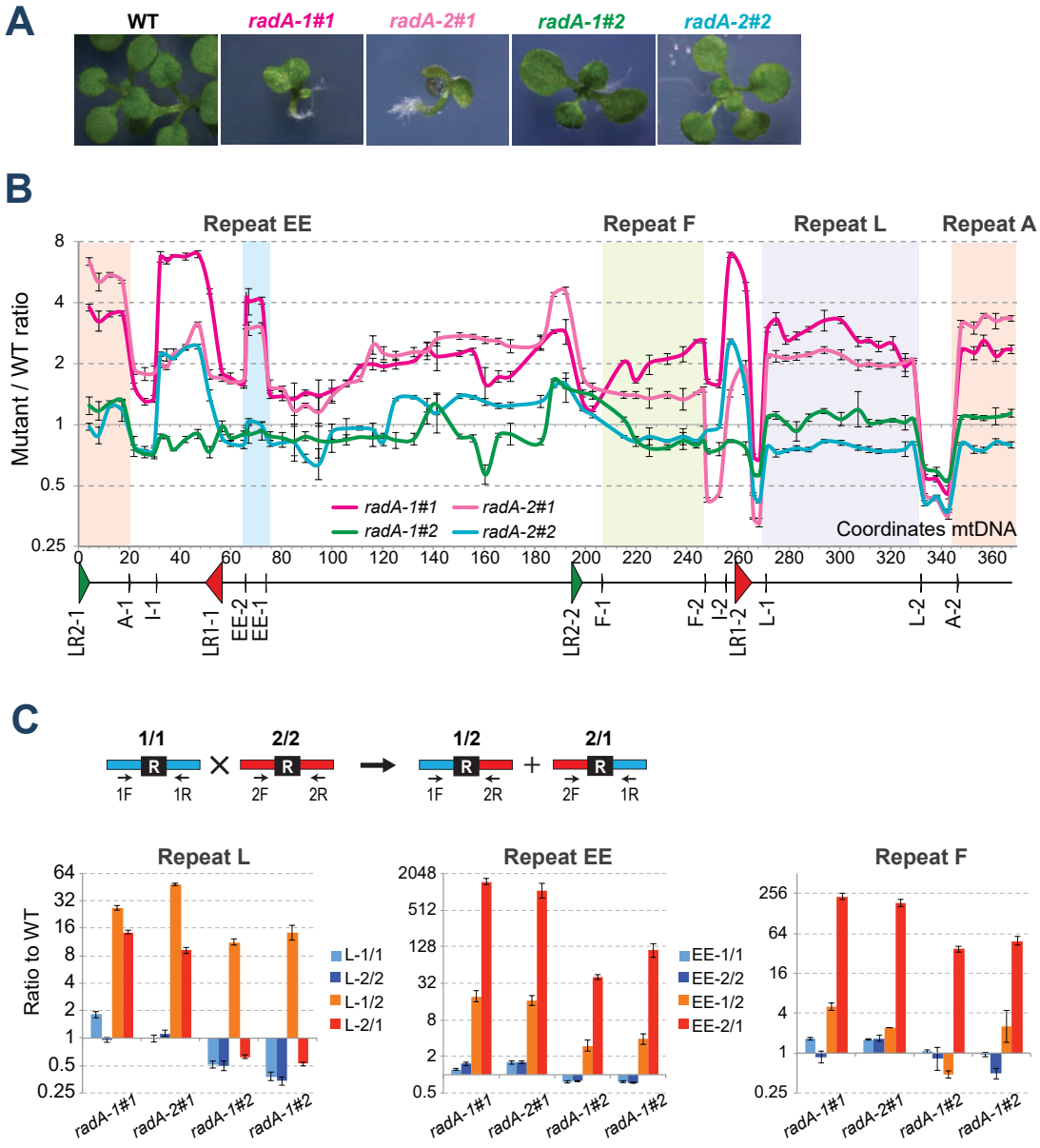

Figure 6. Changes in mtDNA sequences stoichiometry in *radA* mutants because of increased ectopic recombination across repeats.

(**A**) Picture of severely affected (*radA-1*#1 and *radA-2*#1) and mildly affected (*radA-1*#2 and *radA-2*#2) seedlings that were analyzed. (**B**) Scanning of their mtDNA for changes in relative copy numbers of the different mtDNA regions. Sequences spaced 5-10 kb apart on the mtDNA were quantified by qPCR. Coordinates are those of the Col-0 mtDNA sequence. The position of the mtDNA large repeats LR1 and LR2 and of relevant intermediate size repeats are shown below the graphic. Regions with changed stoichiometries flanked by repeat pairs are shadowed. Error bars are the *SD* values from three technical replicates. (**C**) Accumulation of crossover products from mtDNA repeats L, F and EE in the *radA* seedlings relative to WT. Results are in a log2 scale. The scheme shows the qPCR relative quantification of parental sequences 1/1 and 2/2 and of the corresponding crossover products 1/2 and 2/1. Results are the mean of three technical replicates, and error bars correspond to *SD* values.

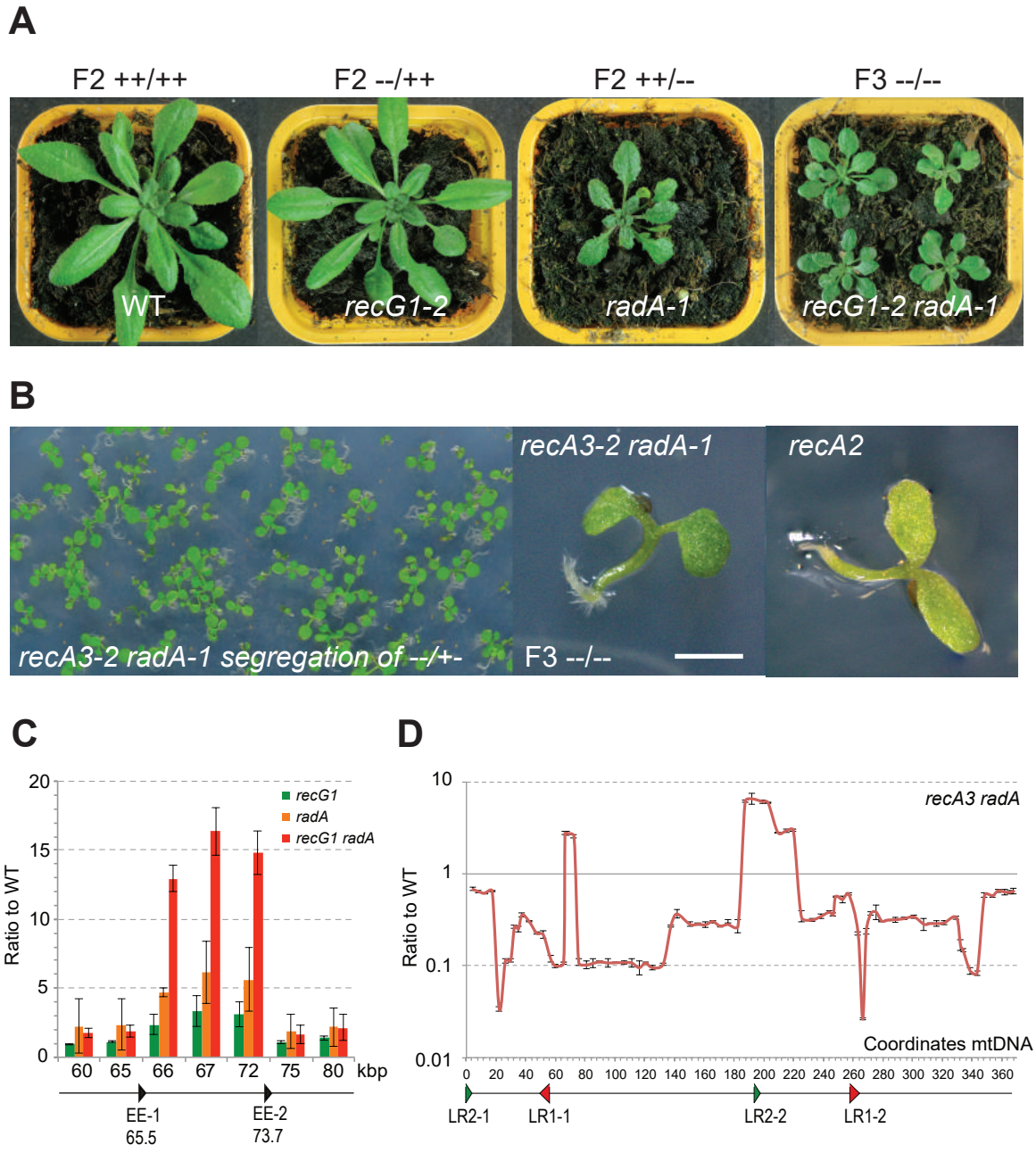

Figure 7. Synergistic effects of the *radA* mutation on *recG1* and *recA3*.
(**A**) Crosses of *recG1-2* and *radA-1* (pollen donor) show that double homozygote *recG1 radA* plants are as affected as simple homozygote *radA* plants. (**B**) Crosses and segregation of *recA3-2* and *radA-1* (pollen donor) show that double homozygote *recA3 radA* seedlings do not grow roots and do not grow further. The phenotype is similar to the one observed for *recA2* mutants (Miller-Messmer et al. 2012). The scale bar is 1 mm. (**C**) qPCR analysis of the copy number of mtDNA sequences around and within the region comprised between pair of repeats EE, previously shown to generate an episome by recombination in *recG1* plants (Wallet et al. 2015). Autonomous replication of the episome is significantly increased in the *recG1 radA* double mutant. Results show the mean and SD error bars from 2 or 3 (for *recG1 radA*) biological replicates. (**D**) Scanning of the copy numbers of the different mtDNA regions in *recA3 radA*, as described in Figure 6, showing severe reduction of several mtDNA regions. Results were compared to those of WT seedling of same size, and are in log scale.

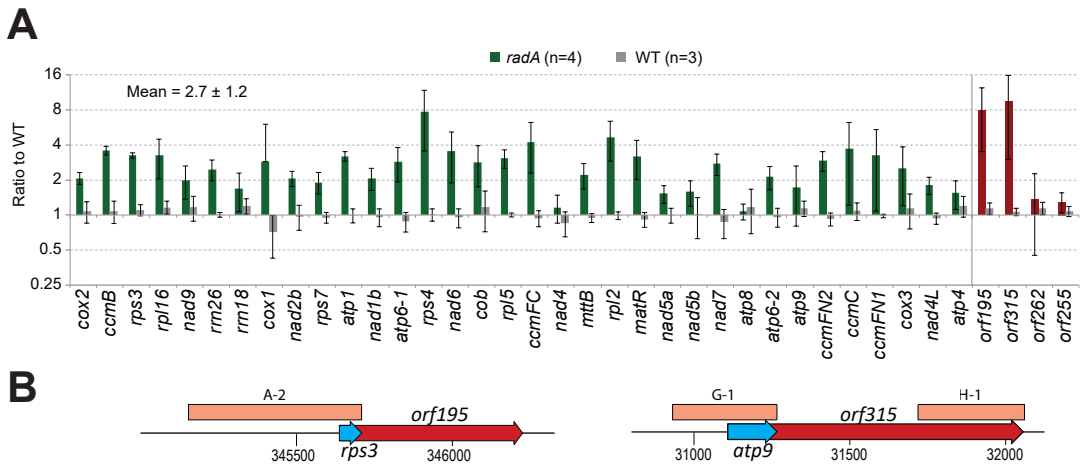

Figure 8. Accumulation of mitochondrial transcripts in *radA*.

(A) Representative mitochondrial transcripts were quantified by RT-qPCR, from the RNA of 10-day old seedlings grown *in vitro,* and normalized against a set of nuclear housekeeping genes. The quantification of several transcripts of orfs whose transcription could be potentially affected by ectopic recombination involving IRs are shown on the right, in red. Results are on a log2 scale and are the mean from four biological replicates (two pools of *radA-1* and two pools of *rad-2* seedlings) and corresponding SD error bars. **(B)** Chimeric *orf195* and *orf315* created by recombination whose transcription is augmented in *radA* plants. The regions corresponding to *rps3* and *atp9* sequences are shown in blue. Repeated sequences are represented by orange bars. Coordinates on the mtDNA are indicated.

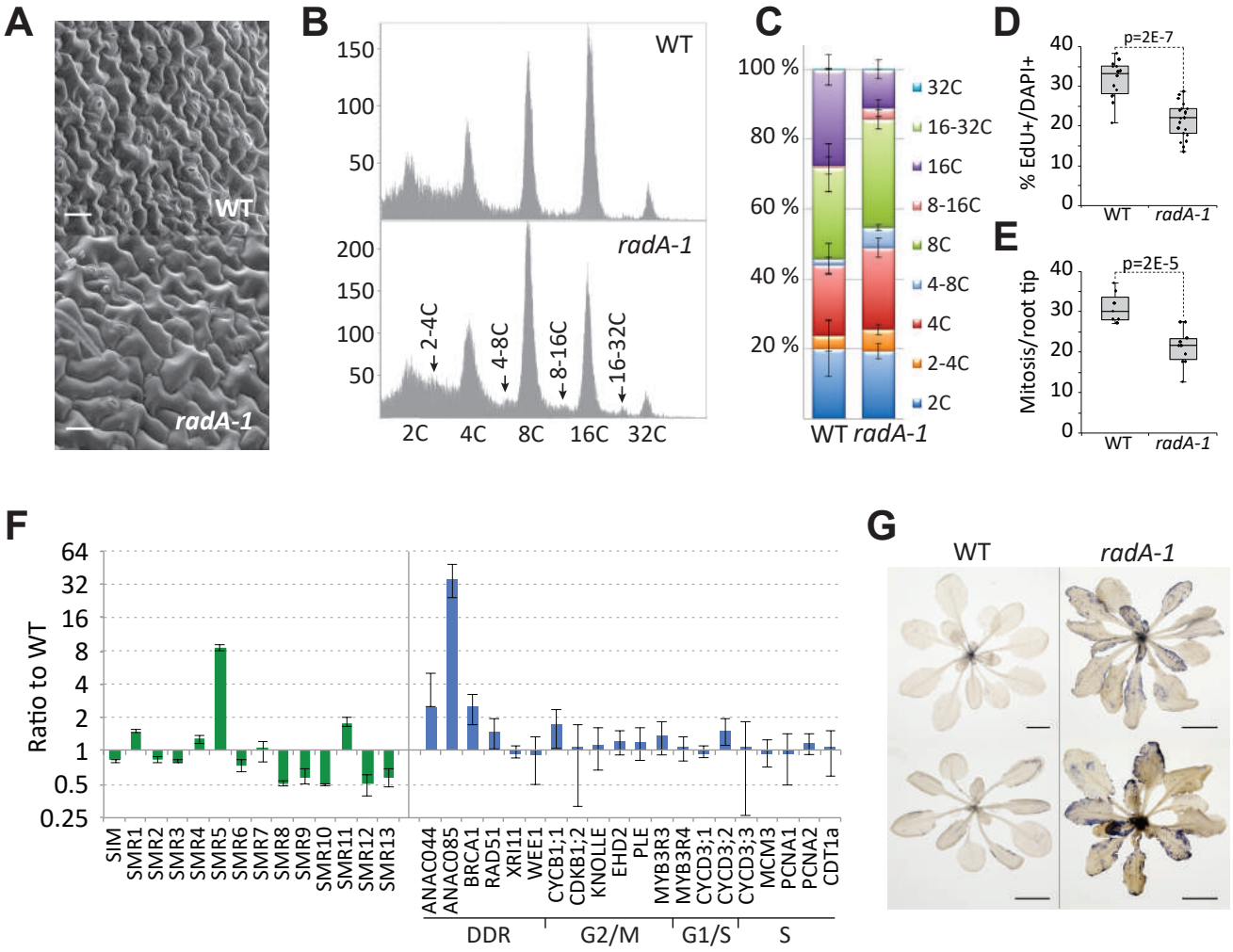

Figure 9. Cell cycle progression is impaired in *radA* plants.

(A) Scanning electron microscopy images showing that in *radA* leaves epidermal cells are much larger and there are fewer stomata, half the number for the same leaf surface. Scale bar is 20 µm. **(B)** Flow-cytometry profile obtained in WT (Col-0) and *radA.* The DNA content of nuclei extracted from the first true leafs of 20 day-old plants was analyzed. **(C)** Ploidy distribution, showing decreased endoreduplication in the mutant, with an increased proportion of 4C and 8C nuclei and a decreased proportion of 16C nuclei. Values are the average ± SD of 4 experiments for WT and six experiments for *radA* (n>20 000 nuclei). **(D)** Decreased DNA synthesis in the nuclei of *radA* root tip cells, as evaluated by the ratio between EdU positive and DAPI (4',6'-diamidino-2-phénylindol) positive cells. **(E)** Decreased number of cells undergoing mitosis. Significances were calculated by Student's t test. **(F)** RT-qPCR analysis of the expression of a set of cell cycle related genes in 10-day old WT and *radA* seedlings, revealing activation of *SMR5* and *ANAC085*. Data is represented in a log2 scale and is the mean ± SE of three biological replicates (two pools of seedlings from *radA-1* and one from *radA-2*). **(G)** NBT (nitro blue tetrazolium) staining for O^{2-} of plants of equivalent size grown under same conditions, showing that *radA* mutants accumulate much more ROS than WT plants. Scale bar is 1 cm.